A STUDY OF RECIPROCATING COMPRESSOR FINGER VALVE DYNAMICS

by

Antonio Spagnuolo, Jr.

Thesis submitted to the Faculty of the

Virginia Polytechnic Institute and State University

in partial fulfillment of the requirements for the degree of

MASTER OF SCIENCE

in

Mechanical Engineering

APPROVED:

R. G. Mitchiner, Chairman

C. E. Knight

R. G. Leonard

December, 1985

Blacksburg, Virginia

STUDY IN THE MODELING OF COMPRESSOR VALVE DYNAMICS

by

Antonio Spagnuolo, Jr.

(ABSTRACT)

The main objective of this research effort was the construction of a finger valve dynamics model using simplified theory based on steady flow conditions. The analytical valve positions were then compared to experimental measurements from an Ingersoll Rand model 242 two-stage air compressor. Proximity probes were used to measure the valve position at two points on the exhaust valve at two different exhaust valve stop heights and at two points on the intake valve at one intake valve stop height in the lower exhaust valve stop height configuration only. A data acquisition system was configured to signal average and digitize the analog data from the sensors using a digital oscilloscope. The data was then sent to and stored in data acquisition computer for future comparisons to analytical results.

The comparisons of the analytical and experimental exhaust valve positions at both points and both valve stop heights were of good quality when the effects of oil stiction were taken into account. Also, the comparisons of the intake valve positions were of good quality after adjustments were made in the theoretical force on the valve calculation. The adjustments entailed accounting for flow induced forces on the intake valve after piston reversal.

Overall the simplified model predicted the valve positions with sufficient quality to warrant the model's use as a design tool.

DEDICATION

This thesis is dedicated to my parents, , Italian immigrants who sacrificed their own ambitions to give their children what my parents never had.

ACKNOWLEDGEMENTS

The author would like to express his sincere appreciation to the following people for their help in this research effort:

Dr. R. G. Mitchiner, his major professor, for his wealth of knowledge, guidance, and his willingness to lend a hand when it was needed.

Dr. R. G. Leonard and Dr. C. E. Knight for serving on his committee.

for his help with the never ending equipment problems.

, his parents, for their gift of freedom of choice.

for her understanding during a rough three months.

The mechanical engineering machine shop for their excellent work and quick service.

TABLE OF CONTENTS

TABLE OF CONTENTS (continued)

LIST OF FIGURES

LIST OF FIGURES (continued)

LIST OF FIGURES (continued

LIST OF TABLES

NOMENCLATURE

A_m	amplitude coefficient for the m^{th} mode
A_p	port area
A_o	bore area
A_v	area under the valve
C_{po}	constant pressure specific heat
C_{vo}	constant volume specific heat
E	modulus of elasticity
g(x)	displacement of the valve at the time of impact with the stop
F_m	generalized force for m^{th} mode
F(t)	force on the valve at time t
F_v	preload on the valve in terms of force
h	valve thickness
I	area moment of inertia
$(KA)_e$	equivalent flow area
K_v	flow coefficient for the valve opening area
L	connecting rod length
ℓ_F	length from fixed end of the valve to the end of the valve port
ℓ_s	length from fixed end of the valve to the start of the valve port
m(t)	generalized mass from m^{th} mode
m_v	mass flow rate through the valve
n	polytropic index
P(x,y,t)	pressure distribution on the valve at time t
$P_c(t)$	cylinder pressure at time t

P_d	downstream pressure
P_u	upstream pressure
Q_A	proportionality constant
R	crank radius
S_H	exhaust valve stop height
t	time
t_b	point in time where valve bouncing occurs
t_H	point in time where the valve hits the stop
t_L	point in time where the valve leaves the stop
t_o	point in time where the valve leaves the seat
T(t)	cylinder temperature at time t
T_o	initial cylinder temperature
$T_n(t)$	participation of n^{th} mode at time t
V(t)	cylinder volume at time t
V_{CL}	cylinder volume at top dead center
w(x,y)	displacement function of the valve
$\dot{w}(x,y)$	velocity function of the valve
$\ddot{w}(x,y)$	acceleration function of the valve
$\underline{w}(x_B)$	displacement of the point x_B along the length of the valve after valve bounding occurs at the point
$\dot{\underline{w}}(x_B)$	velocity of the point x_B along the length of the valve after valve bouncing occurs at the point
W_v	width of the valve
x	point along the length of the valve
x_B	point along the length of the valve where valve bouncing occurs

$x(t)$ position of piston relative to its top dead center position

Greek symbols

∇^2 Laplace operator

ν Poisson's Ratio

$\phi_m(x)$ mode shape function for m^{th} mode

$\psi_m(x)$ mode shape function for n^{th} mode

ω_m m^{th} natural frequency

ρ working fluid density

ρ_o initial density of the working fluid

ρ_v valve material density

γ crank angle

$\dot{\gamma}$ crank angular velocity

ζ_m damping ratio for the m^{th} mode

Transfer Matrix Operators

Note: Subscripts determine the point or field that the variable is referring to. Superscripts determine the side of the point that the variable is referring to. The superscript L refers to the left side of the point and an R the right side.

ℓ length

M moment

V shear

w displacement

θ angular displacement

[F] field matrix

[P] point matrix

1. INTRODUCTION

The valves are one of the most important mechanical components in a compressor are the valves. The proper matching of the valves to the compressor is a key factor in determining the compressor's thermodynamic and mechanical efficiency. Therefore, the valve dynamics need to be included in a compressor simulation model.

The most common types of compressor valves are finger type valves. In its simpliest form the finger type valve is a thin piece of sheet metal (Fig. 1.1). One valve covers each of the entrance and exit ports to the compression chamber, controlling when the working fluid enters and exits the chamber by way of the inlet and outlet plenums, respectively (Fig. 1.2). The exact process of the working fluid entering and leaving the compression chamber can be expressed mathematically as a series of coupled thermodynamic, kinematic, fluid mechanic, and valve dynamics partial differential equations. The exact solution of these simultaneous partial differential equations is difficult if not impossible, and the numerical solution is computationally time consuming. Therefore, a simplified but valid compressor model is required for feasible analytical compressor development. Since finger type valves are common and they add complexity to the simulation model, the main thrust of this research effort is the development of simplified models for finger valve dynamics.

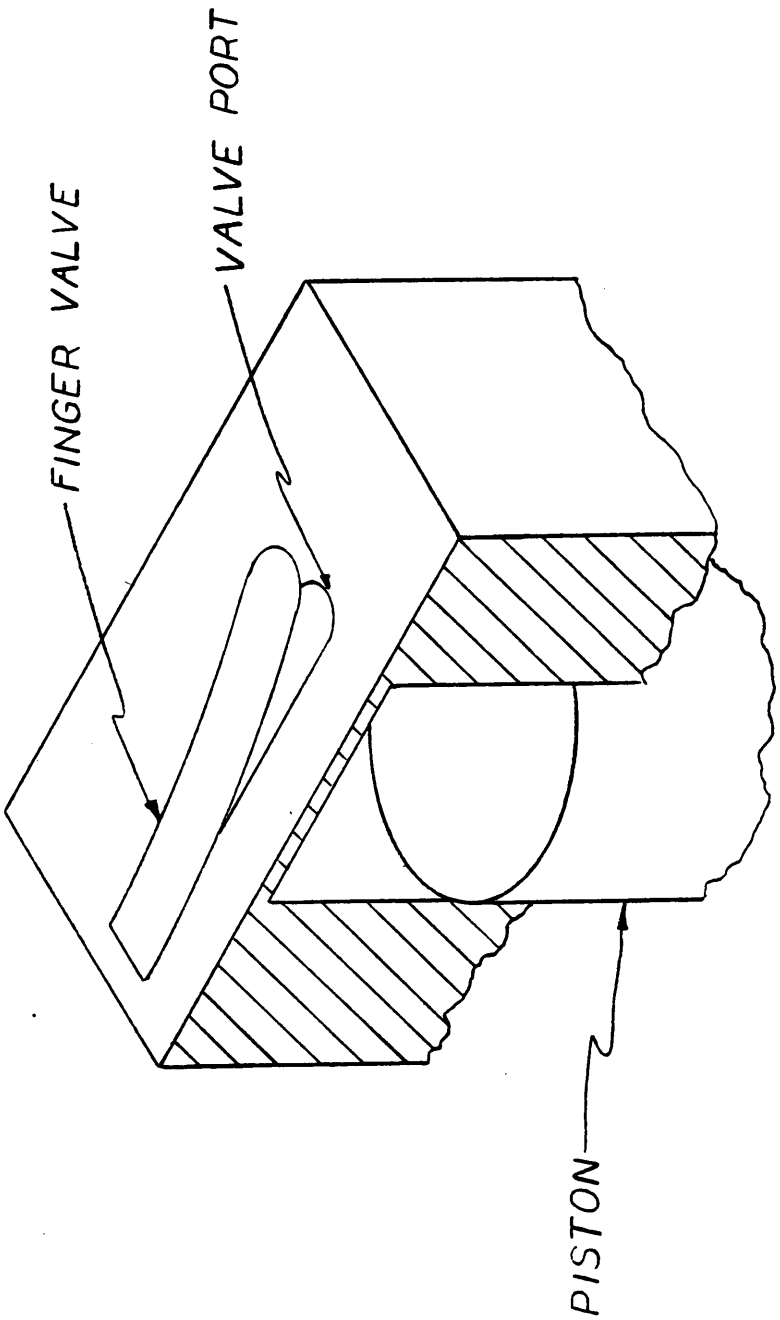

Figure 1.1: A reciprocating compressor finger valve.

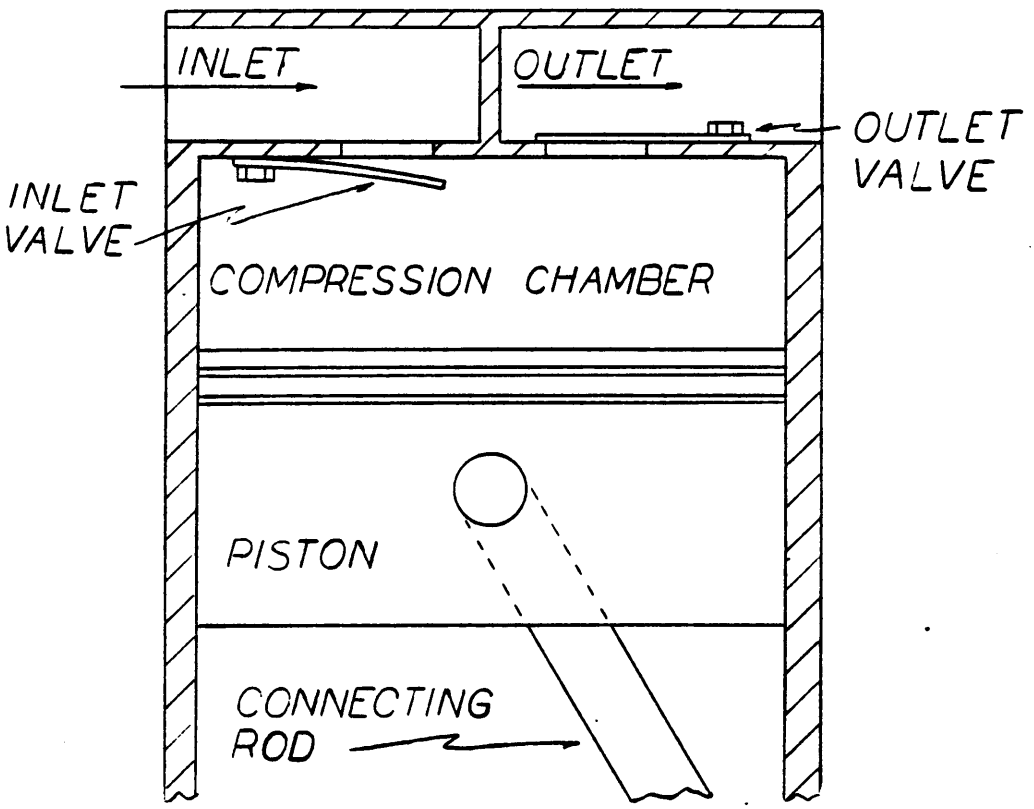

Figure 1.2: A basic reciprocating compressor.

The order of progression in this research effort is as follows:

1. Development of the simplifed compressor model.
2. Computer implementation of the model.
3. Experimental verification of the model.

The final goal of this research effort is to develop a valve model that can be used in a compressor model so that the cylinder pressures and valve positions can be accurately predicted.

2. LITERATURE REVIEW

Costagliola [1] produced the first meaningful mathematical model of a compressor and its valves in 1950. Corresponding experimental work was on a single cylinder air compressor. Although the experimental and analytical results were not directly compared, Castagliola claimed the model to be essentially correct. However, at that time the non-linear differential equations proved to be too tedious to solve for use in industrial applications.

With the emergence and wide availability of digital computers, the complicated mathematical model derived by Castagliola [1] became feasible to solve. Two early works using models based on Castagliola's work were those by MacLaren and Kerr [2], and Wambsgnass and Cohen [3].

In the MacLaren and Kerr study, the following conclusions were made:

1. That oil between the valve and valve seat causes a delay in the valve opening time. This phenomena is called "oil stiction".
2. That a compressor simulation program can produce results faster and cheaper than an experimental analysis.

It should be noted that the MacLaren and Kerr simulation program depended on experimental results in order to determine the coefficients necessary to calculate the mass flow rate and force on the valve.

In the first of many works performed at Purdue University, Wambgnass and Cohen [3] made a comparison between the analytical and experimental analysis of a 1/4 H.P., 3600 RPM, hermitically sealed, single cylinder air compressor. The correlation was judged good when

taking into account the instrumentation problems associated with the small compressor. The Wambgnass and Cohen model treated the valves as a multi-degree-of-freedom system rather than a single degree-of-freedom system as in earlier approaches. The single degree-of-freedom system was concluded to be too simple to adequately describe the valve motion in high-speed compressors. Also, it was found that damping and valve stiction played a significant role in modeling valve motion. As in the MacLaren and Kerr [2] study, Wambgnass and Cohen required experimental data to calculate the mass flow rate and force on the valve analytically.

With Wambgnass's and Cohen's [3] initial work, extensive work was done on the development of mathematical models during the late 1960's and early 1970's at Purdue University. Soedel [4] produced a manual summarizing this work. The manual detailed the necessary thermodynamic, kinematic, fluid mechanic, and valve dynamic equations to produce a compressor model. A computer simulation incorporating these equations compared well to experimental results. However, the model required experimental data to calculate the coefficients necessary to calculate the mass flow rate and the forces on the valves.

In an extension to the Soedel text [4], Hamilton [5] produced a similiar document with alternatives to all the equations presented in the Soedel text. Of interest is the analytical method to calculate the mass flow rates and the force on the valve, which in previous works required experimental data. The method used to calculate the mass flow rate assumes incompressible flow. The method for calculating the force assumes steady flow conditions and that the flow changes direction by

90° upon meeting the valve. Testing the force calculation method, Hamilton made the following observations:

1. The method is valid for "small" valve displacements.
2. The method works well under normal flow conditions (i.e., flow is into the compressor chamber when the intake valve is open), and produces significant error during back flow (i.e., flow is out of the compression chamber when the intake valve is open).

Gatecliff, and Lady [6] presented a method to solve the forced vibration differential equation of a finger valve of uniform thickness and non-uniform width. The method uses a Rayleigh-Ritz procedure to provide an approximate solution to the exact formulation of the differential equation. Comparing one point on the valve, the analytical method produced a valve cycle of the same shape as that of the true valve, however, actual displacements were not compared due to experimental difficulties.

Papastegious et al. [7] used finite element methods and the experimentally measured pressure drop across the valve to determine the motion of the valve. Comparing a static and a dynamic finite element analysis, the static analysis underpredicted the valve displacement and associated stresses by up to three and five times, respectively.

Gatecliff, Griner, and Richardson [8] presented analytical results of a simplified compressor simulation program. In this effort, the valve is modeled as a series of lumped masses connected by massless beams. Richardson, Gatecliff, and Griner [9] verified the results from the simplified model. Only physical parameters such as valve closing

time, valve opening time, and cylinder pressure were compared with excellent results.

Giacomelli and Giorgetti [10] performed an experimental study on the phenomena of oil stiction, which causes a delay in valve opening time. The findings indicate that the delay is significant enough to cause a significant error in an analytical program if not taken into account.

From the literature summarized in the previous paragraphs, the following observations can be made:

1. The use of compressor simulation programs is a valuable development tool.

2. Valve damping and oil stiction are important factors in determining valve motion.

3. Many of the analytical compressor model tested to date require experimental data.

4. That analysis of valve dynamics using the Finite Element Method is time prohibitive.

3. THEORETICAL DEVELOPMENT

The theoretical development of the compressor model is presented in the sections to follow.

3.1 Valve Dynamics

The equation of motion for a finger type compressor valve begins with the plate bending equation as presented by Soedel [4]. For the plate element in Fig. 3.1, the plate bending equation is presented below:

$$\left[\frac{E\,h^3}{12(1-\nu^2)}\right] \nabla^4 w(x,y) + \rho_v h \ddot{w}(x,y) = P(x,y,t) \tag{3.1}$$

where

E = modulus of elasticity

h = valve thickness

ρ_v = density of valve material

ν = Poisson's ratio

$w(x,y)$ = valve displacement at point (x,y) (Fig. 3.1)

$P(x,y,t)$ = Pressure on the valve at point (x,y) at time t

and

$$\nabla^4 = \frac{\partial^4}{\partial x^4} + 2\,\frac{\partial^4}{\partial x^2 \partial y^2} + \frac{\partial^4}{\partial y^4} \tag{3.2}$$

In Soedel [4] the valve displacement function, $w(x,y)$, is described in terms of a weighted sum of the valves natural modes, as shown below:

$$w(x,y) = \sum_{m=1}^{\infty} q_m(t)\,\phi_m(x,y) \tag{3.3}$$

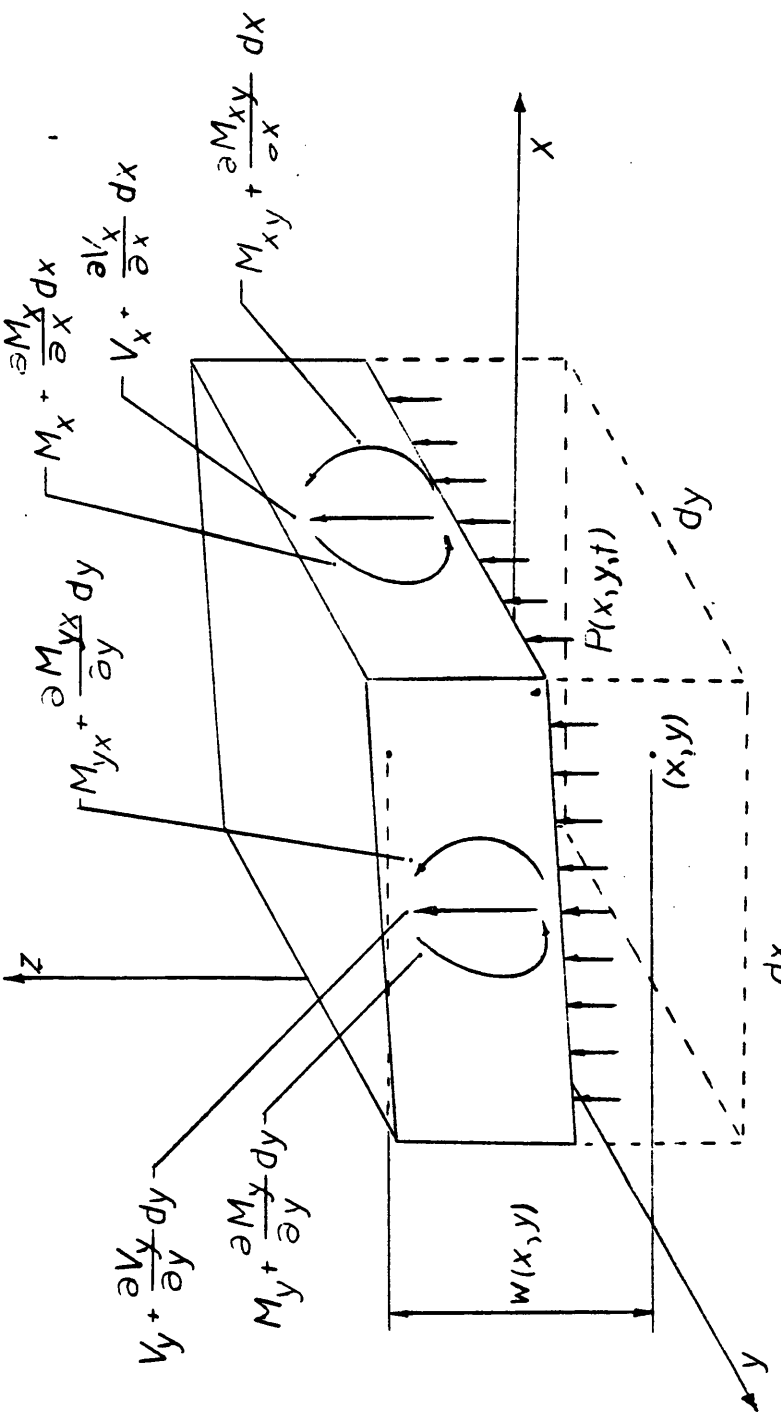

Figure 3.1: Free body diagram of a plate element.

where

$q_m(t)$ = participation factor for the m^{th} mode at time t

$\phi_m(x,y)$ = m^{th} mode shape function

utilizing Eq. (3.3), Eq. (3.2) becomes

$$\left[\frac{E\,h^3}{12(1-\nu^2)}\right]\left(\sum_{m=1}^{\infty} q_m(t)\nabla^4\phi_m(x,y)\right) + \rho_v h\left(\sum_{m=1}^{\infty} \ddot{q}_m(t)\,\phi_m(x)\right) \qquad (3.4)$$

$$= P(x,y,t).$$

In the free vibration state P(x,y,t) is zero and Eq. (3.1) becomes

$$\left[\frac{E\,h^3}{12(1-\nu^2)}\right]\nabla^4 w(x,y) + \rho_v h\,\ddot{w}(x,y) = 0 \qquad (3.5)$$

If the valve is freely vibrating in its m^{th} mode, w(x,y) can be expressed as follows:

$$w(x,y) = A_m\,\phi_m(x,y)\,\sin\omega_m t. \qquad (3.6)$$

where

A_m = amplitude coefficient

ω_m = natural circular frequency of the m^{th} mode.

Substituting Eq. (3.6) into Eq. (3.5) results in the following equation:

$$\ddot{w}(x,y) = - \omega_m^2 \, w(x,y) \tag{3.7}$$

Substituting Eq. (3.7) into Eq. (3.4) yields

$$\nabla^4 = \frac{12 \, \rho_v h \, \omega_m^2 (1-\nu^2)}{E \, h^3} \tag{3.8}$$

Substituting Eq. (3.8) into Eq. (3.4) yields

$$\sum_{m=1}^{\infty} \omega_m^2 \, q_m(t) \, \phi_m(x,y) + \sum_{m=1}^{\infty} \ddot{q}_m(t) \, \phi_m(x,y) = \frac{P(x,y,t)}{\rho_v h} \tag{3.9}$$

To reduce Eq. (3.9) the following orthogonality property from reference [13] is utilized:

$$\iint_s \phi_m(x,y) \, \phi_n(x,y) \, dxdy = \begin{cases} 0 & m \neq n \\ \iint_s \phi_m^2 (x,y) & m = n \end{cases} \tag{3.10}$$

where

$\iint_s$ = integration over the entire surface

Therefore, Eq. (3.9) becomes

$$\ddot{q}_m(t) + \omega_m^2 \, q_m(t) = \frac{\iint_s P(x,y,t) \, \phi_m(x,y) dxdy}{\rho_v h \iint_s \phi_m^2 \, dxdy} \tag{3.11}$$

$$m = 1,2,3 \ldots . \infty$$

Reducing Eq. (3.11) and (3.3) to a one dimensional case produces the following equations:

$$\ddot{q}_m(t) + \omega_m^2 q_m(t) = \frac{\int_L P(x,t)\ \phi_m(x)dx}{\rho_v h \int_L \phi_m^2(x)dx} \qquad (3.12)$$

$$m = 1,2,3 \ldots . \infty$$

and

$$w(x) = \sum_{m=1}^{\infty} q_m(t)\ \phi_m(x) \qquad (3.13)$$

where

$\int_L$ = intergration over the valve length

x = point along the length of the valve

The term in the numerator on the right side of the equality in Eq. (3.12) is commonly called the generalized force, F_m, and the denominator; the generalized mass, M_m. With these simplification Eq. (3.12) becomes

$$\ddot{q}_m(t) + \omega_m^2 q_m(t) = \frac{F_m}{M_m} \qquad m = 1,2,3 \ldots .\infty \qquad (3.14)$$

where

$$F_m = \int_L P(x,t)\ \phi_m(x)dx \qquad (3.15)$$

and

$$M_m = \rho_v h \int_L \phi_m^2(x)dx \tag{3.16}$$

Although there is very little damping internal to the valve material, Hamilton [5] reports that previous experimental investigations have correlated the valve damping to the valve velocity. Hamilton further states that this damping arises from the working fluid interacting with the valve. Hamilton accounts for the damping by including an equivalent modal damping, as follows:

$$\ddot{q}_m + \zeta_m \omega_m \dot{q}_m(t) + w_m^2 q_m(t) = \frac{F_m}{M_m} \quad m = 1,2\ 3\ .\ .\ .\ .\ \infty \tag{3.17}$$

where ζ_m is the damping factor for the m^{th} mode.

The solution of the valve dispacement function, w(x), per Eq. (3.13) requires the solution of an infinite number of differential equations in the form of Eq. (3.17). In actuality only the lower modes are required to solve w(x) with reasonable accuracy. This will be elaborated upon in later sections.

The solution of Eq. (3.17) requires both the natural modes and the pressure function P(x,t). The determination of both quantities will be discussed in later sections after the boundary conditions of the valve are treated.

3.1.1 Treatment of Valve Boundary Conditions

The ideal valve opens and closes quickly and experiences small displacements yielding small stresses and a corresponding long fatigue

life, however, quick response and small displacements are competing valve features. A quick acting valve requires a low valve stiffness and small displacements require a large valve stiffness. Therefore, most compressors have valve stops (Fig. 3.2) that limit the maximum displacement of a low stiffness valve to produce an ideal valve (quick acting and small displacements). However, valve stops complicate the valve dynamics since the stops cause nonlinear boundary conditions. Modeling the nonlinear boundary conditions require the mathematical treatment of the following elastic configurations:

1. The valve leaves the seat.
2. The valve hits the stop and stays at the stop.
3. The valve leaves the stop and returns to the seat.
4. The valve bounces on a hard surface.

When the valve leaves the seat at time, t_o, the valve is at rest. The initial conditions for Eq. (3.17) are, therefore, as follows:

$$\begin{aligned} q_m(t_o) &= 0 \\ \dot{q}_m(t_o) &= 0 \end{aligned} \qquad m = 1,2,3 \ldots \infty \tag{3.18}$$

The boundary conditions for the valve in this elastic configuration are fixed at one end and free at the other.

At time t_m when the valve hits and stays at the stop, the boundary conditions change to fixed at one end and hinged at the other. The displacement of the valve is now the superposition of the valve

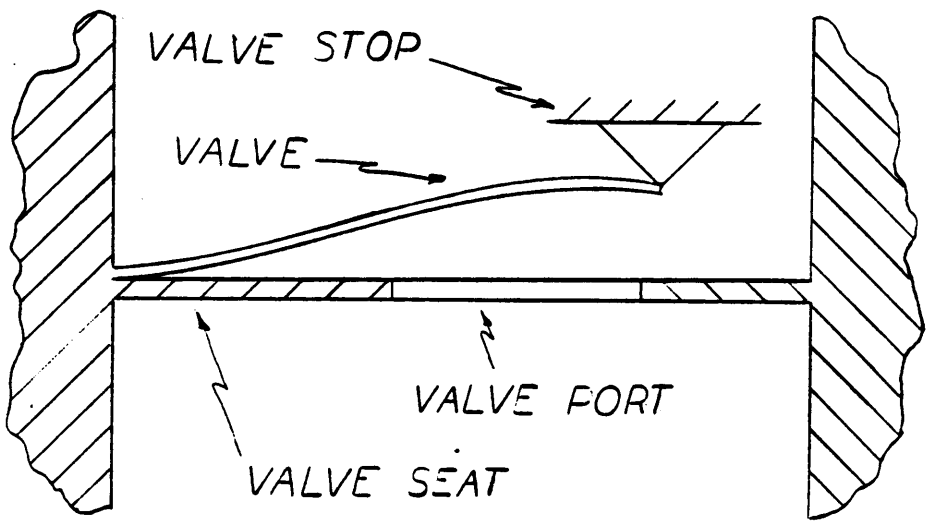

Figure 3.2: A valve stop for a finger valve.

displacement at time t_H, g(x), plus any further displacement. This is displayed graphically in Fig. 3.3 and mathematically below:

$$w(x,t>t_H) = g(x) + \sum_{n=1}^{\infty} T_n(t)\ \psi_n(x) \tag{3.19}$$

where

$\psi_n(x)$ = n^{th} mode shape function of the new boundary conditions.

$T_n(t)$ = participation factor for n^{th} mode of the new boundary conditions.

and

$$g(x) = \sum_{m=1}^{\infty} q_m(t_H)\ \phi_m(x) \tag{3.20}$$

Placing Eq. (3.19) and (3.20) into Eq. (3.1) and repeating the steps that produced Eq. (3.17) yields the following equation:

$$\ddot{T}_n(t) + \zeta_n \omega_n \dot{T}_n(t) + \omega_n^2\ T_n(t) = \frac{F_n}{M_n} - \frac{\sum_{m=1}^{\infty} q_m(t_H)\ w_m^2 \int_L \phi_m(x)\ \psi_n(x)}{\int_L \psi_n^2(x)}$$

$$m = 1,2,3 \ldots . \infty,\ t > t_H \tag{3.21}$$

where

$$F_n = \int_L P(x,t)\ \psi_n(x)dx \tag{3.22}$$

$$M_n = \rho_v h \int_L \psi_n^2(x)\ dx \tag{3.23}$$

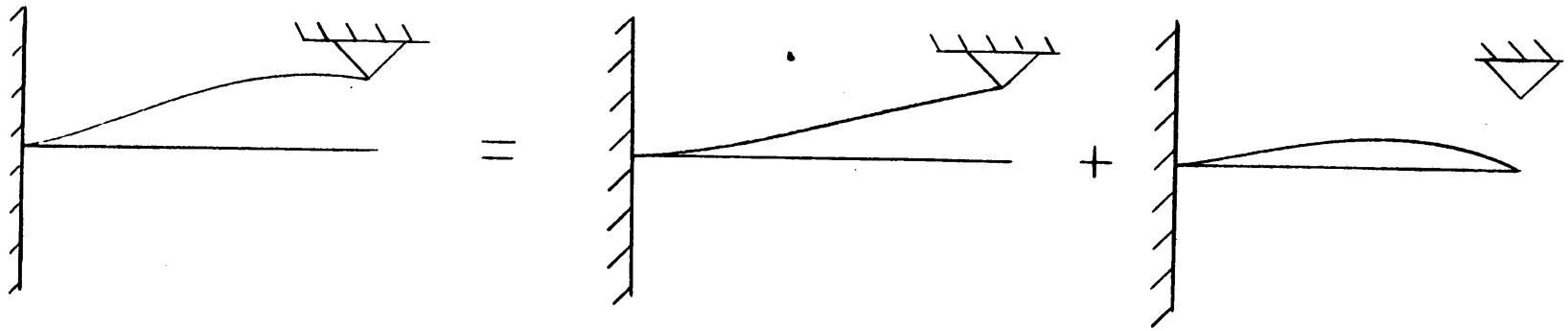

$$W(X, t > t_H) = g(X) + \sum_{n=1}^{\infty} T_n(t)\,\psi_n(X)$$

Figure 3.3: Superposition of the valve displacement after the valve hits the stop.

and

w_n = n^{th} natural frequency of the valve under its new boundary conditions

ζ_n = damping ratio for the nth mode

The solution of the series of equations in the form of Eq. (3.21) yields the valve displacement function from Eq. (3.19) when $t > t_H$.

The initial conditions for Eq. (3.21) are obtained by equating displacements and velocities of the new and old boundary conditions at time t_H. Equating displacements

$$\sum_{m=1}^{\infty} q_m(t_H)\phi_m(x) = g(x) + \sum_{n=1}^{\infty} T_n(t_H)\psi_n(x) \tag{3.24}$$

Substituting Eq. (3.20) into Eq. (3.24) yields

$$T_n(t_H) = 0 \quad n = 1,2,3 \ldots \infty \tag{3.25}$$

Equating velocities

$$\sum_{m=1}^{\infty} \dot{q}_m(t_H)\ \phi_m(x) = \sum_{m=1}^{\infty} \dot{T}_n(t_H)\ \psi_n(x) \tag{3.26}$$

using the orthogonal properties shown in Eq. (3.10)

$$\dot{T}_n\ (t_H) = \frac{\sum_{m=1}^{\infty} \dot{q}_m(t_H) \int_L \phi_m(x)\ \psi_n(x)dx}{\int_L \psi_n^{\,2}(x)\ dx} \quad n = 1,2,3 \ldots \infty \tag{3.27}$$

The valve leaves the stop and returns to the seat at time t_L when the pressure force is less than the dynamic and elastic forces. Stated in equation form, the valve returns to the seat when the following inequality is true:

$$\sum_{n=1}^{\infty} \ddot{T}_n(t)\psi_n(x) + \sum_{n=1}^{\infty} \zeta_n w_n \dot{T}_n(t)\psi_n(x) + \sum_{n=1}^{\infty} w_n^2 T_n(t)\phi_n(x) + \sum_{n=1}^{\infty} \omega_m^2 q_m(t_H)\phi_m(x) > \frac{P(x,t)}{p_v h} \tag{3.28}$$

At the time t_L, the valves boundary conditions return to fixed at one end and free at the other. The initial conditions are again found by equating displacments and velocities, yielding

$$q_m(t_L) = g(x) + \frac{\sum_{n=1}^{\infty} T_n(t_L) \int_L w_n^2 \phi_m(x)\psi_n(x)dx}{\int_L \phi_m^2(x)\, dx} \tag{3.29}$$

$$m = 1,2,3 \ldots \infty$$

$$\dot{q}_m(t_L) = \frac{\sum_{n=1}^{\infty} \dot{T}_n(t_L) \int_L \phi_m(x)\psi_n(x)dx}{\int_L \phi_m^2(x)dx} \tag{3.30}$$

$$m = 1,2,3 \ldots \infty$$

Valve bouncing occurs when a point x_b on the valve impacts and bounces off a hard surface, such as the valve stop or seat. When valve bouncing occurs at time t_B, the velocity, $\dot{w}(x_b)$, of the point of impact is reversed in direction and decreased in magnitude (Eq. 3.31), and the

points position, $\omega(x_B)$, is held to the position of the obstruction (Eq. 3.32).

$$\underline{\dot{w}}(x_B) = - C_r \quad \dot{w}(x_B) \tag{3.31}$$

$$\underline{w}(x_B) = Y_o \tag{3.32}$$

where

$\underline{\dot{w}}(x_B)$ = velocity of point x_B after impact.

C_r = coefficient of restitution.

$\dot{w}(x_B)$ = velocity of point x_B before impact.

$\underline{w}(x_B)$ = the new position of the point x_B.

Y_o = the position of the obstruction.

New participation factors that correctly describe the new displacement and velocity functions of the valve, $\underline{w}(x)$ and $\underline{\dot{w}}(x)$, respectively are required. Applying the orthogonality principles presented in Eq. (3.10), the new participation factors are calculated as follows:

$$\underline{q}_m(t_B) = \frac{\int_L \underline{w}(x)\ \phi_m(x)dx}{\int_L \phi_m^2(x)dx} \qquad m = 1,2,3 \ldots \infty \tag{3.33}$$

$$\underline{\dot{q}}_m(t_B) = \frac{\int_L \underline{\dot{w}}(x)\ \phi_m(x)dx}{\int_L \phi_m^2(x)dx} \qquad m = 1,2,3 \ldots \infty \tag{3.34}$$

where

$\underline{w}(x)$ = the displacement function of the valve after impact

$\dot{\underline{w}}(x)$ = the velocity function of the valve after impact.

$\underline{q}_m(t_B)$ = participation factor of the m^{th} mode after impact

$\dot{\underline{q}}_m(t_B)$ = derivative of the participation factor for the m^{th} mode after impact.

3.1.2 Determination of the Pressure on the Valve

Hamilton [5] presents a method to calculate the pressure function, P(x,t), which is necessary for the solution of Eq. (3.17). Hamilton defines the force on the valve in Fig. 3.4 as follows:

$$F(t) = \frac{\dot{m}_v^2}{2\rho_v}\left(\frac{A_p}{(K_v A_v)^2} + \frac{1}{A_o}\right) - F_v \qquad (3.35)$$

where

$\dot{m}_v$ = mass flow rate through the valve

ρ = density of the working fluid

A_p = port area

A_o = bore area

A_v = area under the valve

K_v = flow coefficient for the area under the valve

F_v = elastic preload on the valve in terms of force

Hamilton made the following assuptions in deriving Eq. (3.35):

1. The valve displacements are small.
2. The flow changes direction by 90° as it meets the valve.
3. The flow is steady.
4. The flow is stagnated at the valve opening.

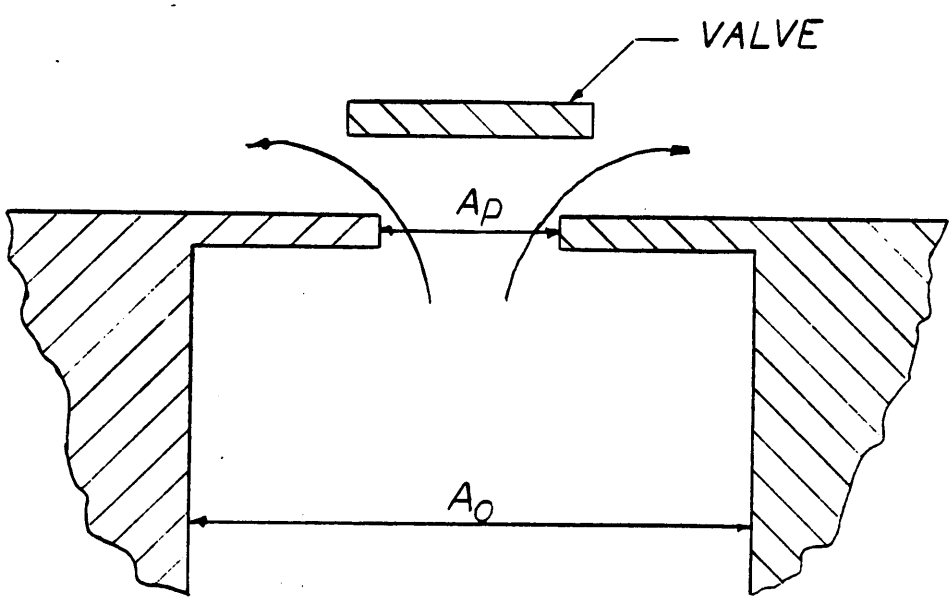

Figure 3.4: Display of the physical parameters used in the force on the valve calculation.

A simplified mass flow rate equation is presented by Hamilton [5]. Hamilton assumes that each flow system in a compressor may be modeled as a system of orifices. Therefore, the following equation for flow through an orifice may be used:

$$\dot{m}_v = (KA)_e \, Y \sqrt{2\rho \, (P_d - P_u)} \tag{3.36}$$

$\dot{m}_v$ = mass flow rate through the valve

$(KA)_e$ = equivalent flow area for the valve system

Y = compressibility factor

ρ = working fluid density

P_d = downstream pressure

Pu = upstream pressure

Hamilton then assumes the fluid is incompressible ($Y = 1$), and goes on to develop equations to calculate $(KA)_e$. Since in this research effort the working fluid is air, the incompressible assumption is invalid. However, in most compressors the greatest obstruction to the flow occurs at the valve. Therefore, it is assumed the equivalent flow area for the flow system is approximately the equivalent flow area under the valve. Expressed mathematically

$$(KA)_e \simeq K_v A_v \tag{3.37}$$

utilizing Eq. (3.36)

$$\dot{m}_v = (K_v A_v Y) \sqrt{2\rho (P_d - P_u)} \tag{3.38}$$

and

$$F(t) = (K_v A_v Y)^2 \left(\frac{A_p}{(K_v A_v)^2} + \frac{1}{A_o}\right)(P_d - P_u) - F_v \tag{3.39}$$

Assuming that the pressure distribution is constant over the valve length that covers the valve port in Fig. 3.5.

$$P(x,t) = \begin{cases} \dfrac{F(t)}{(\ell_F - \ell_s) w_v} & \ell_s < x < \ell_F \\ 0 & x < \ell_x \text{ , } x > \ell_F \end{cases} \tag{3.40}$$

The generalize force, F_m, in Eq. 3.15, therefore becomes

$$F_m = \frac{F(t)}{(\ell_F - \ell_s) w_v} \int_{\ell_s}^{\ell_F} \varphi(x) dx \tag{3.41}$$

where P(t) is calculated by Eq. (3.39). In order to utilize Eq. (3.39) and (3.38) the pressure drop across the valve must be known. This will be treated in a later section.

3.2 Determination of the Free Vibration Modes of the Compressor Valves

The valve dynamics equations developed in Section 3.1 require the natural frequencies and mode shapes of the valves at their various boundary conditions. In the past, the natural modes have been found experimentally or by the finite element method. The finite element

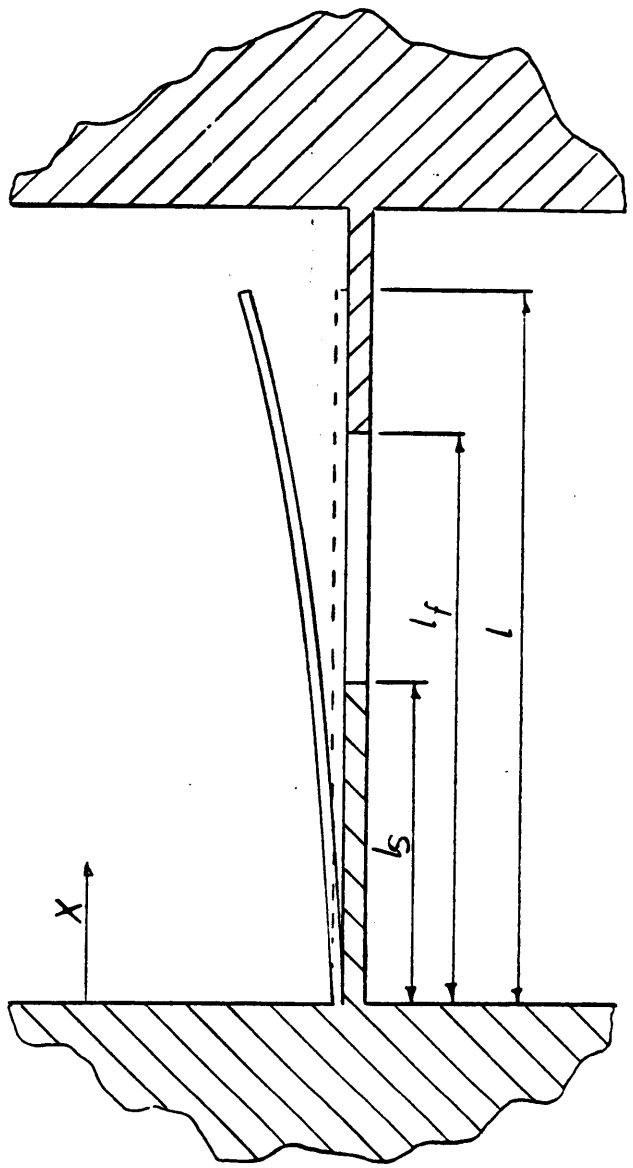

Figure 3.5: Definition of the limits used in integrating the pressure on the valve function.

method has the disadvantage of considerable difficulties in interfacing the finite element program with the compressor simulation program. Experimental determination of the mode shapes is typically hampered by the valves small size. Also, experimental methods require time, facilities, and physical parts; all disadvantages for the analytical development of a compressor model. An alternative method is the transfer matrix method.

Since finger valves are commonly thin pieces of sheet metal of constant cross-sectional area, the valve can be modeled as a series of lumped masses connected by massless beams (Fig. 3.6). With such a model the transfer matrix method can be used to determine the bending natural modes.

As Thomson [12] presents the transfer matrix method, the method is ideal for lumped parameter systems made of several subsystems. The method formulates a matrix that solves the state (displacement and forces) of one end of the subsystem knowing the state of the other end. The combination of the matrices of each subsystem of a total system yields a matrix that describes the total system.

To determine the natural modes of the valve modeled in Fig. 3.6 by the transfer matrix method, the matrices describing a point mass and a massless beam are required. The matrices are called field and point matrices for the massless beam and point mass, respectively. The field matrix and point matrix label indicate whether the subsystem has length or not, respectively.

The matrices are derived using the free body diagrams of the point mass and the massless beam shown in Fig. 3.7. The subscripts indicate

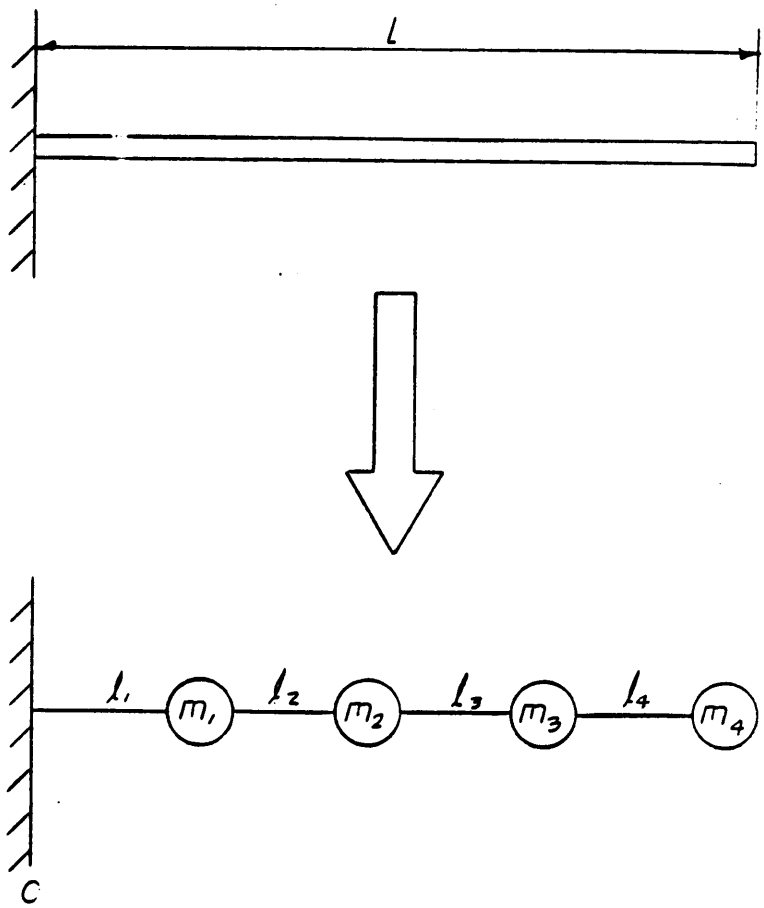

Figure 3.6: Lumped mass model of a finger valve.

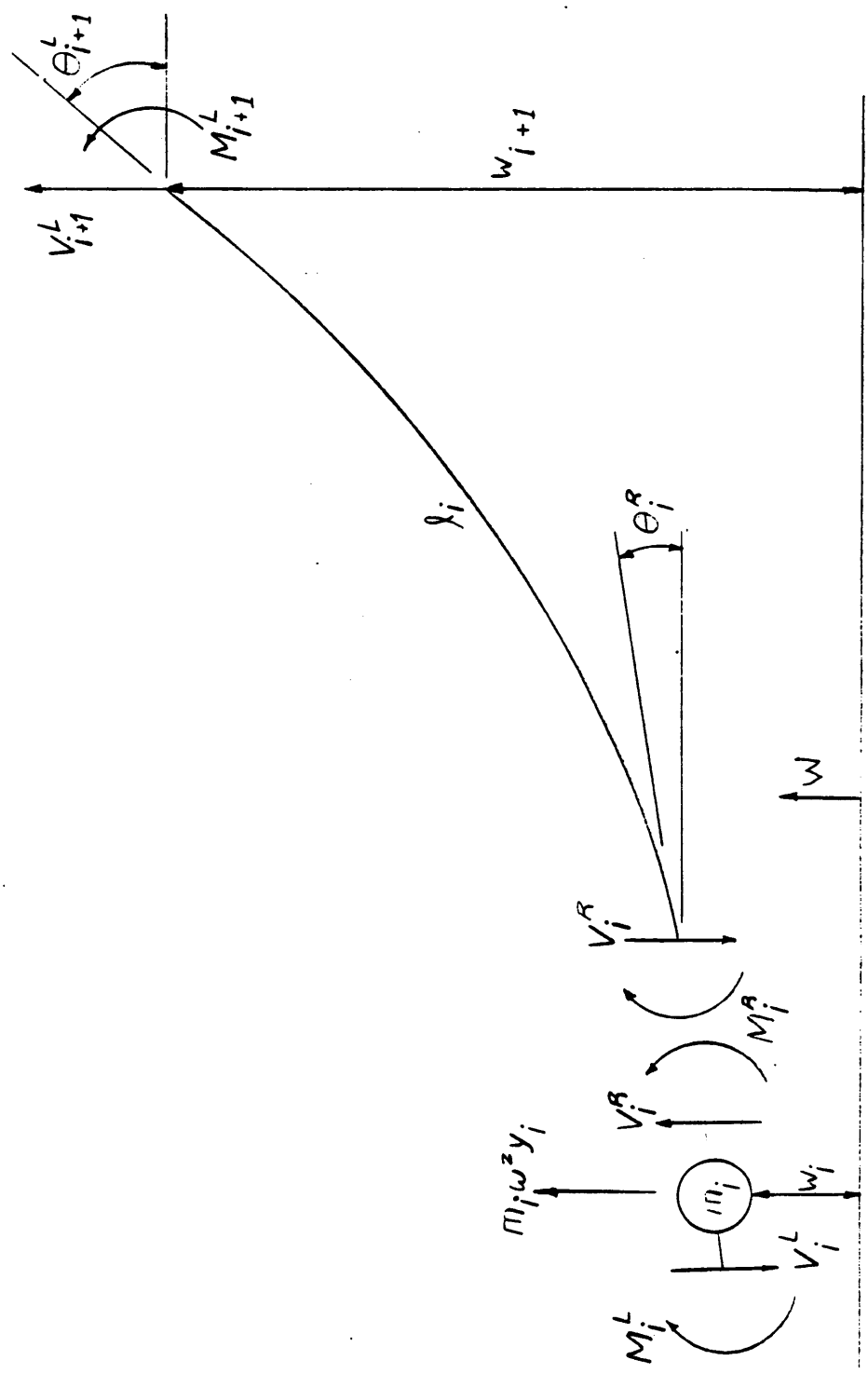

Figure 3.7: Free body diagram of a point mass and a massless beam.

the point or field to which the variable is associated and the superscript, the side of the point. The superscript L is for the left side of the point and R, the right side.

Thomson [12] writes the following equations from the free body diagram of the massless beam in Fig. (3.7)

$$V_{i+1}^{L} = V_{i+1}^{R} \tag{3.42}$$

$$M_{i+1}^{L} = M_{i}^{R} - V_{i}^{R}\, \ell_i \tag{3.43}$$

$$\theta_{i+1}^{L} = \theta_{i}^{R} + M_{i+1}^{L} \left(\frac{\ell}{EI}\right)_i + V_{i+1}^{L} \tag{3.44}$$

$$w_{i+1}^{L} = w_{i}^{R} + \theta_{i}^{R}\ell_i + M_{i+1}^{L} \left(\frac{\ell^2}{2EI}\right)_i + V_{i+1}^{L}\left(\frac{\ell^3}{3EI}\right)_i \tag{3.45}$$

where

V = shear

M = moment

ℓ = beam length

E = modulus of elasticity

I = area moment of inertia

θ = angular beam deflection

w = displacement

Substituting Eqs. (3.42) and (3.43) into Eq. (3.44) and (3.45) and arranging into matrix form

$$\begin{Bmatrix} -V \\ M \\ \theta \\ w \end{Bmatrix}^{L}_{i+1} = \begin{bmatrix} 1 & 0 & 0 & 0 \\ \ell & 1 & 0 & 0 \\ \ell^2/2EI & \ell/EI & 1 & 0 \\ \ell^3/6EI & \ell^2/2EI & \ell & 1 \end{bmatrix}_i \begin{Bmatrix} -V \\ M \\ \theta \\ w \end{Bmatrix}^{12}_{i} \tag{3.46}$$

The column vectors are known as state vectors, and the four by four matrix is known as the field matrix, $[F]_i$, for the i^{th} beam.

Thomson [12] repeats the same process for the point mass in Fig. 3.7 and yields the following matrix equation:

$$\begin{Bmatrix} -V \\ M \\ \theta \\ w \end{Bmatrix}^{R}_{i} = \begin{bmatrix} 1 & 0 & 0 & m\omega^2 \\ 0 & 1 & 0 & 0 \\ 0 & 0 & 1 & 0 \\ 0 & 0 & 0 & 1 \end{bmatrix}_i \begin{Bmatrix} -V \\ M \\ \theta \\ w \end{Bmatrix}^{12}_{i} \tag{3.47}$$

where

ω = circular excitation frequency.

The four by four matrix is the point matrix, $[P]_i$, for a point mass.

Substituting matrix Eq. (3.47) into matrix Eq. (3.46) yields

$$\begin{Bmatrix} -V \\ M \\ \theta \\ w \end{Bmatrix}^{R}_{i+1} = \begin{bmatrix} 1 & 0 & 0 & m\omega^2 \\ \ell & 1 & 0 & m\omega^2\ell \\ \ell^2/2EI & \ell/EI & 1 & m\omega^2\ell^2/EI \\ \ell^3/6EI & \ell^2/2EI & \ell & \left(1 + \frac{m\omega^2\ell^2}{6EI}\right) \end{bmatrix}_i \begin{Bmatrix} -V \\ M \\ \theta \\ w \end{Bmatrix}^{L}_{i} \tag{3.48}$$

The resulting four by four matrix is the transfer matrix since it transfers the i^{th} state vector into the $i+1^{th}$ state vector.

For the valve model shown in Fig. 3.6, the transfer matrix model is produced by successive multiplications of field and point matrices, as shown below:

$$\begin{Bmatrix} -V \\ M \\ \theta \\ w \end{Bmatrix}_4^R = [P]_4[F]_4[P]_3[F]_3[P]_2[F]_2[P]_1[F]_1 \begin{Bmatrix} -V \\ M \\ \theta \\ w \end{Bmatrix}_0 \tag{3.49}$$

Letting

$$[P]_4[F]_4[P]_3[F]_3[P]_2[F]_2[P]_1[F]_1 = \begin{bmatrix} u_{11} & u_{12} & u_{13} & u_{14} \\ u_{21} & u_{22} & u_{23} & u_{24} \\ u_{31} & u_{32} & u_{33} & u_{34} \\ u_{41} & u_{42} & u_{43} & u_{44} \end{bmatrix} \tag{3.50}$$

Matrix Eq. (3.49) becomes

$$\begin{Bmatrix} -V \\ M \\ \theta \\ W \end{Bmatrix}_4^R = \begin{bmatrix} u_{11} & u_{12} & u_{13} & u_{14} \\ u_{21} & u_{22} & u_{23} & u_{24} \\ u_{31} & u_{32} & u_{33} & u_{34} \\ u_{41} & u_{42} & u_{43} & u_{44} \end{bmatrix} \begin{Bmatrix} -V \\ M \\ \theta \\ W \end{Bmatrix}_0 \tag{3.51}$$

The boundary conditions for the model in Fig. 3.6 are

$$\left.\begin{aligned} M_4^R &= 0 \\ V_4^R &= 0 \\ \theta_o &= 0 \\ w_o &= 0 \end{aligned}\right\} \tag{3.52}$$

Applying the boundary conditions to matrix Eq. (3.51) yields

$$\begin{bmatrix} u_{11} & u_{12} \\ u_{21} & u_{22} \end{bmatrix} \begin{Bmatrix} -V \\ M \end{Bmatrix}_0^R = \begin{matrix} 0 \\ 0 \end{matrix} \tag{3.53}$$

Since

$$\begin{Bmatrix} -V \\ M \end{Bmatrix}_0^R = 0 \tag{3.54}$$

for only the trivial solution of Eq. (3.53), which is when there is no motion of the valve,

$$\text{DET} \begin{vmatrix} u_{11} & u_{12} \\ u_{21} & u_{22} \end{vmatrix} = 0 \tag{3.55}$$

The solution of Eq. (3.53) yields the natural frequencies. The mode shapes are then found by solving for the displacement, w, for each point at each of the natural frequencies.

In order to ascertain the accuracy of the transfer matrix method, the method was compared to the solution of Thomson's [13], Euler's Equation for beams and results from a finite method analysis of a beam with dimensions (1.24) cm x (.1969) cm x (5.906×10^{-3}) cm. In the transfer matrix method analysis, the beam was modeled as 20 successive and equal massless beam-point mass elements. In the finite element

method solution the beam was modeled with 40 rectangular shell elements using the code ANSYS [14]. The comparision of the first three bending natural frequencies is shown in Table 1, and the comparison of the mode shapes is shown in Figs. 3.8-3.10.

Since all three methods have underlying assumptions and inaccuracies that cause their results to deviate from the true modes, the only conclusion that can be made is that the transfer matrix method yields results comparable to other commonly accepted methods.

Although the transfer matrix method has been displayed for only two types of subsystems, point masses and massless beams, Pestel and Leckie [15] show many more cases where the transfer matrix can be used. The use of the transfer matrix method can be used to analyze a multitude of elastomechanical systems, and the method's capabilities are only dependent on the enthusiasm of the analyst.

Table 1: Comparison of the Calculated Bending Natural Frequencies

Mode	Transfer Matrix Method (Hz)	Euler's Equation (Hz)	Finite Element Method (Hz)
1	47.05	49.45	49.90
2	295.25	309.08	314.50
3	827.71	866.85	888.13

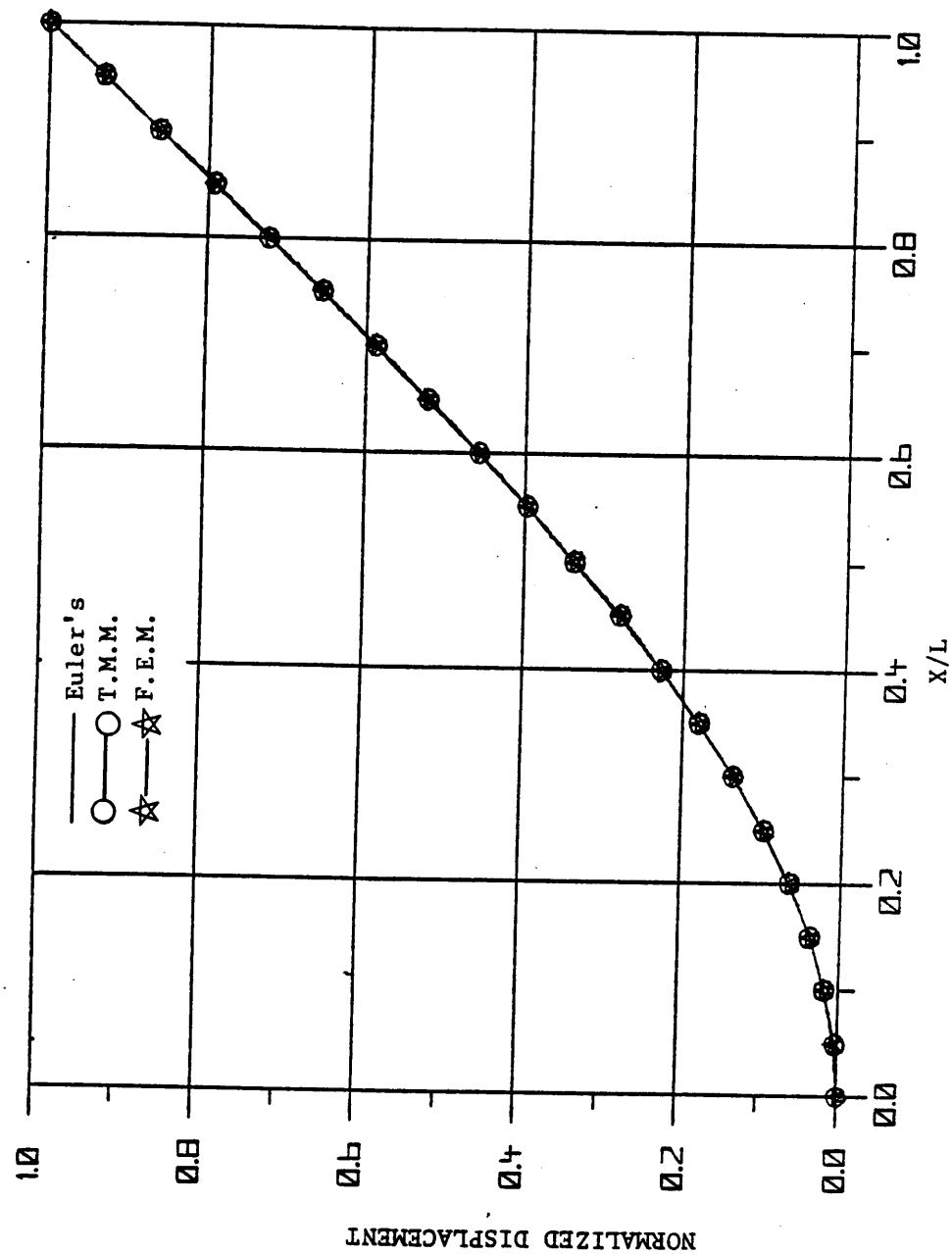

Figure 3.8. Comparison of the First Mode Shapes Obtained from Euler's Euqation, the Transfer Matrix Method (T.M.M.) and the Finite Element Method (F.E.M.).

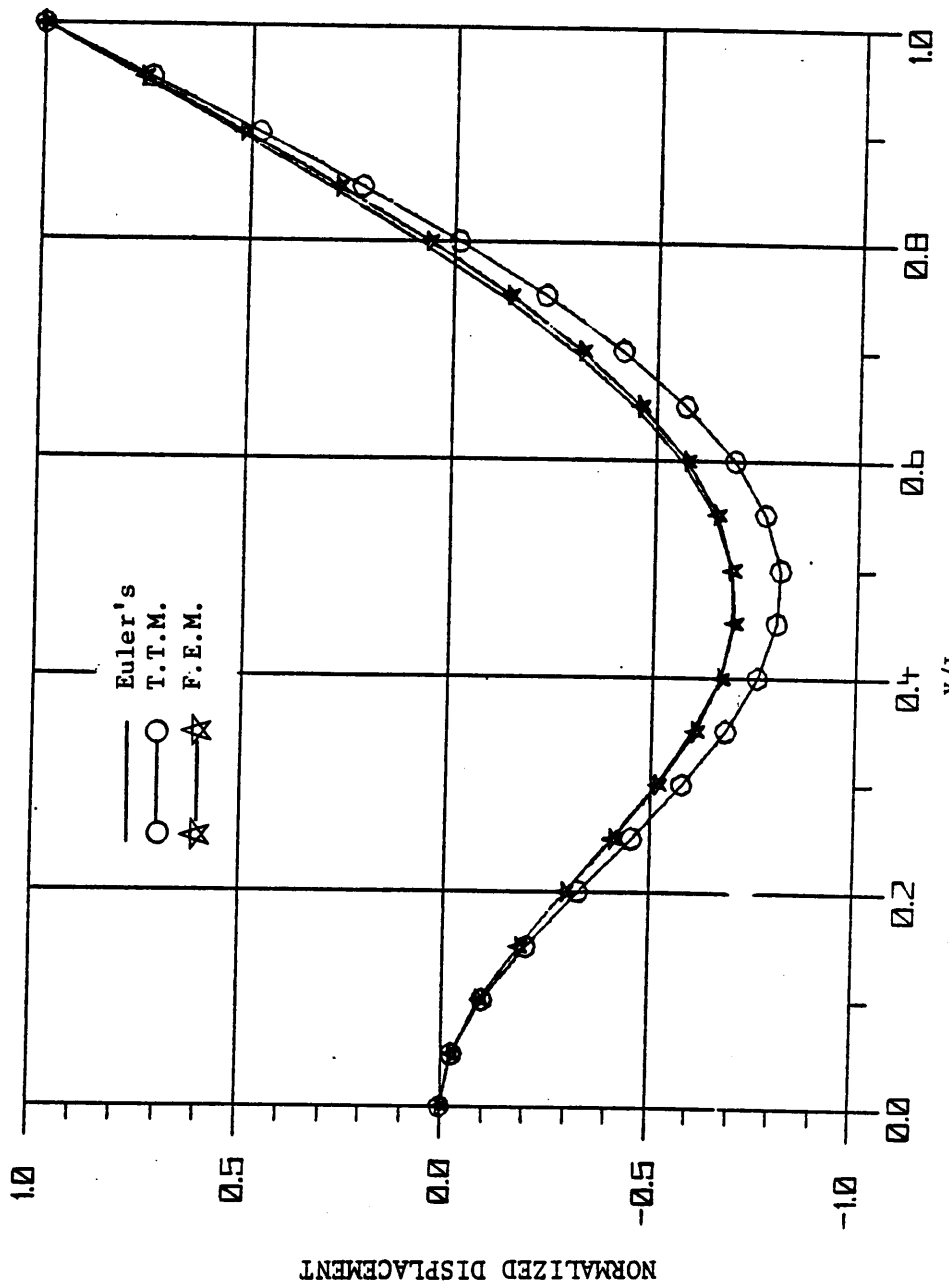

Figure 3.9. Comparison of the Second Mode Shapes Obtained from Euler's Equation, the Transfer Matrix Method (T.M.M.), and the Finite Element Method (F.E.M.).

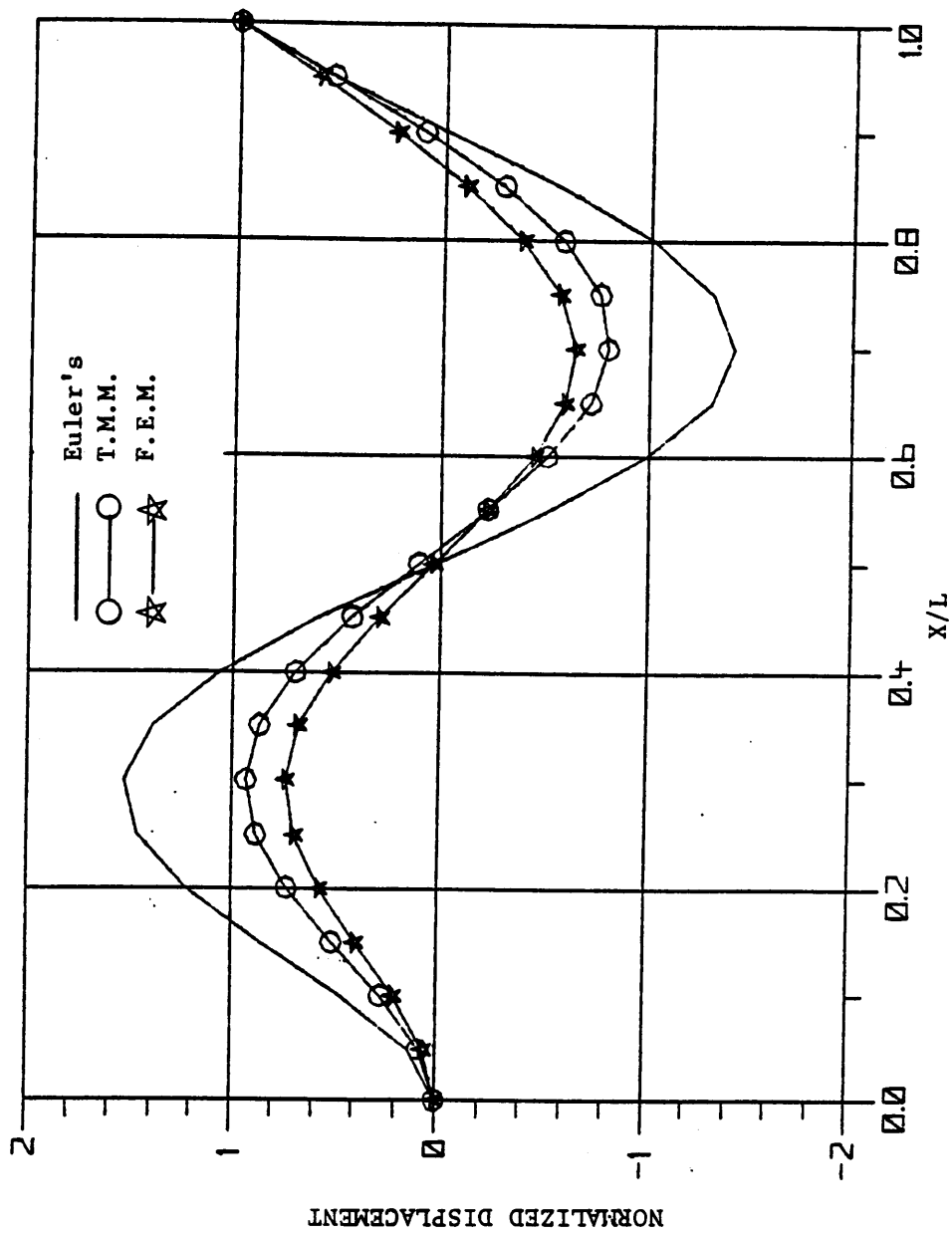

Figure 3.10. Comparison of the Third Mode Shapes Obtained from Euler's Equation, the Transfer Matrix Method (T.M.M.), and the Finite Element Method (F.E.M.).

3.3 Compression Chamber Thermodynamics

As stated earlier the pressures on each side of each valve are required. Therefore, the cylinder pressure is required.

For many simple compression and expansion processes the pressure volume relationship of Eq. (3.54) is valid. Such processes are

$$PV^n = \text{constant} \tag{3.54}$$

where

P = pressure

V = volume

n = polytropic index

called polytropic processes. The plot of the logarithm of pressure versus the logarithm of volume for such a process is a straight line of slope n (Fig. 3.11). The value of n depends on the type of thermodynamic process. For an isothermal process n=1, and for an adiabatic process n is commonly described as follows:

$$n = \frac{C_{po}}{C_{vo}} \tag{3.55}$$

where

C_{po} = constant-pressure specific heat

C_{vo} = constant-volume specific heat

Assuming that the thermodynamic cycle in a compressor undergoes is polytropic, the following equations may be used to calculate the cylinder temperature and pressure at time t:

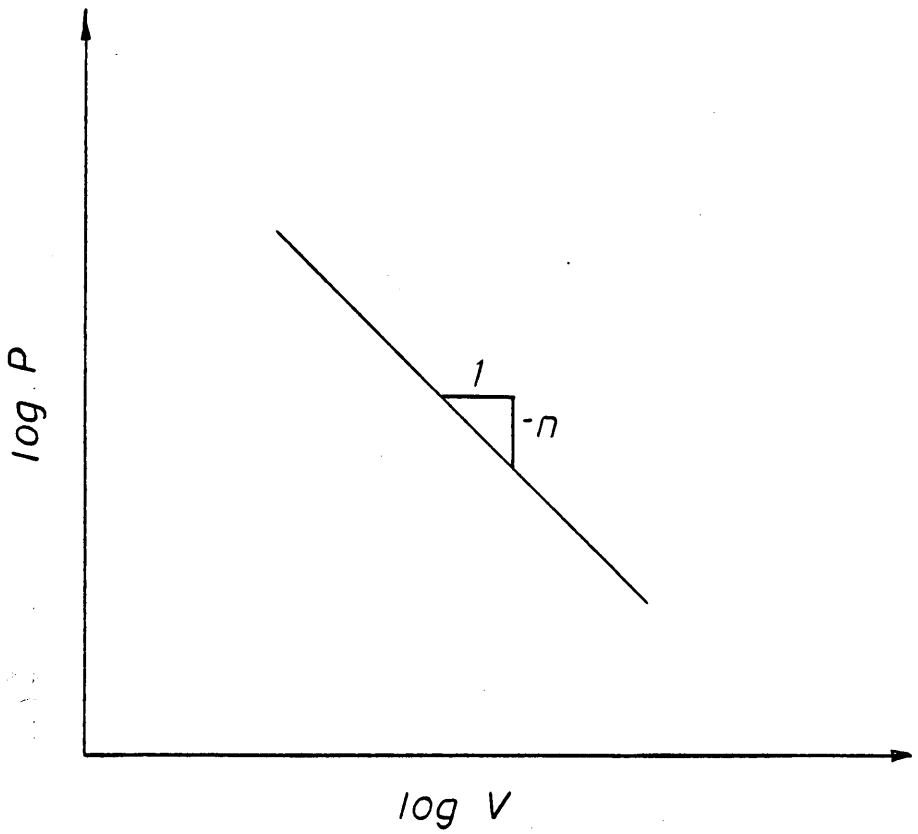

Figure 3.11: Log P vs. log V plot for a polytropic process.

$$P_c(t) = P_o \left(\frac{m(t)}{\rho_o V(t)}\right)^n \tag{3.56}$$

$$T(t) = T_o \left(\frac{P(t)}{P_o}\right)^{\frac{n-1}{n}} \tag{3.57}$$

where

$P_c(t)$ = cylinder pressure at time t

$T(t)$ = cylinder temperature at time t

$V(t)$ = cylinder volume

$m(t)$ = mass in the cylinder at time t

ρ_o = initial density of the working fluid

P_o = initial cylinder pressure

T_o = initial cylinder temperature

The mass flow rate shown in Eq. (3.38) is used to determine m(t), and the cylinder volume calculation is presented in the next section.

3.3.1 Cylinder Volume Calculation

The cylinder volume for the simple compressor shown in Fig. 3.12 is calculated as follows:

$$V(t) = X(t) \cdot A_o + V_{CL} \tag{3.58}$$

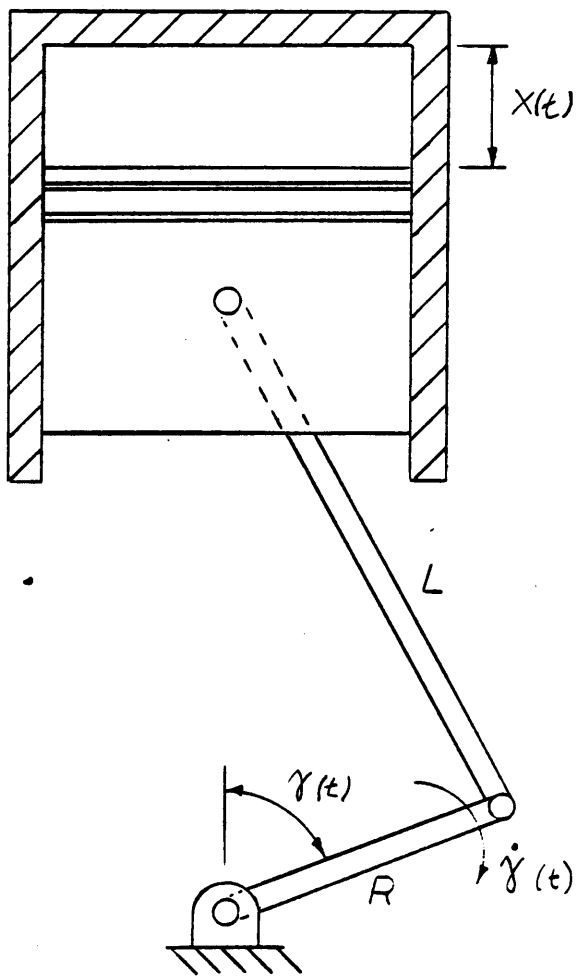

Figure 3.12: The basic kinematic components of a single cylinder compressor.

where

$X(t)$ = piston position relative to top dead center

A_o = cylinder bore area

V_{CL} = cylinder volume at top dead center

The position of the piston with respect to top dead center, $X(t)$, (Fig. 3.12) is presented by Mabie and Ocvirk [16],

$$X(t) = - R \cos \gamma - [L^2 - R^2 \sin^2 \gamma]^{1/2} + (R + L) \qquad (3.59)$$

where

R = crank radius

L = connecting rod length

γ = crank angle

Assuming a constant speed compressor, the crank angle, γ, is calculated as follows:

$$\gamma = \dot{\gamma} t \qquad (3.60)$$

where

$\dot{\gamma}$ = crank angular speed.

t = time

4. VERIFICATION OF THE MATHEMATICAL MODEL

Model verification was performed by writing a computer program that incorporated the compressor theory presented in Chapter 3, then comparing the program's results to measurements made on an actual compressor.

4.1 Experimental Measurements

Experimental data was obtained from the first stage of an Ingersoll Rand Model 242 two-stage air compressor. The physical parameters measured were exhaust valve positions at two points on the valve, the intake valve positions at two points, the cylinder pressure, and the exit plenum pressure. The exhaust valve and intake valve positions were measured at the points shown in Figs. 4.1 and 4.2, respectively. Appendix A details the methods used in acquiring the data.

The exhuast valve positions at the two points, the cylinder pressure, and exit plenum pressure were measured at two different exhaust valve stop heights, S_H (Fig. 4.4). The stop height was changed by changing the gasket thickness between the first stage cylinder head and the valve plate as shown in Fig. 4.3 (the exhaust valve stop is an integral part of the cylinder head). The two exhaust valve stop heights, S_H, were .35 mm and 1.0 mm, respectively. The intake valve stop height was 1.65 mm in both cases. The intake valve position was not measured in the higher exhaust valve stop height configuration due to experimental limitations.

It is noted that the first stage of the Ingersoll Rand Model 242 compressor has two identical intake and two identical exhaust valves. The position of only one valve of each set was measured.

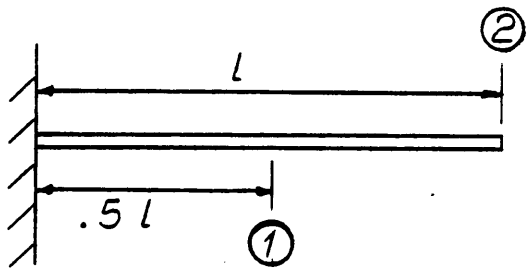

Figure 4.1: Points on the exhaust valve where the valve positions were expermentially measured.

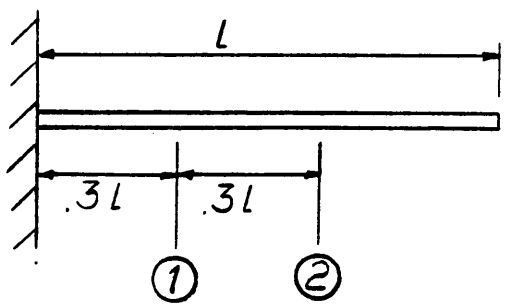

Figure 4.2: Points on the intake valve where the valve positions were expermentially measured.

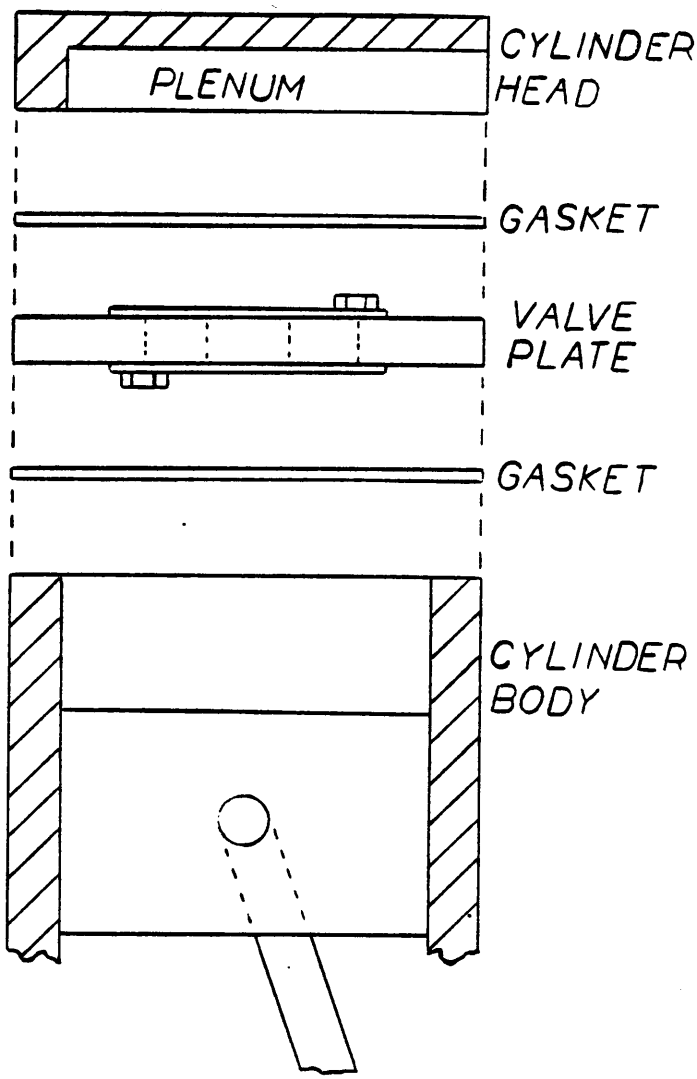

Figure 4.3: Basic setup of the Ingersoll-Rand Model 242 compressor.

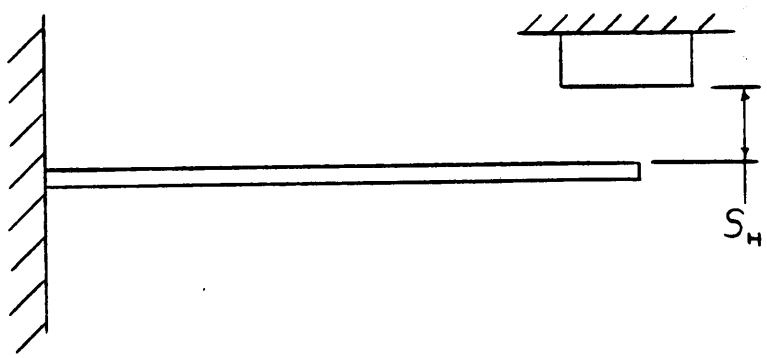

Figure 4.4: Definition of the valve stop height.

4.2 Compressor Simulation Program

Using the theory presented in Chapter 3, a single stage compressor simulation program was written. The flow chart of the program is shown in Fig. 4.5. As seen in Fig. 4.5, the program has two basic modes of operation: using experimentally measured cylinders pressures, or using the theory presented in Section 3.2 to calculate the cylinder pressure. The ability to use measured cylinder pressures was incorporated to test the valve dynamics theory free of any errors induced by the analytical cylinder pressure calculation.

Since the simulation program is for a single stage compressor, the experimentally measured first stage exit plenum pressures were used in the program to take into account the second stage of the Model 242 compressor. The theory presented in Chapter 3 is not limited to a single stage compressor, but the program was limited to a single stage for the following reasons:

1. The extension of the program to two stages made theoretical deficiencies too difficult to solve.
2. To limit computer run time.

For clarity the assumptions made in the theory presented in Chapter 3 are repeated below:

1. The pressure is constant over the portion of the valve that covers the valve port (Fig. 3.5), and zero every where else.
2. The thermodynamic process in the compression chamber is polytropic.

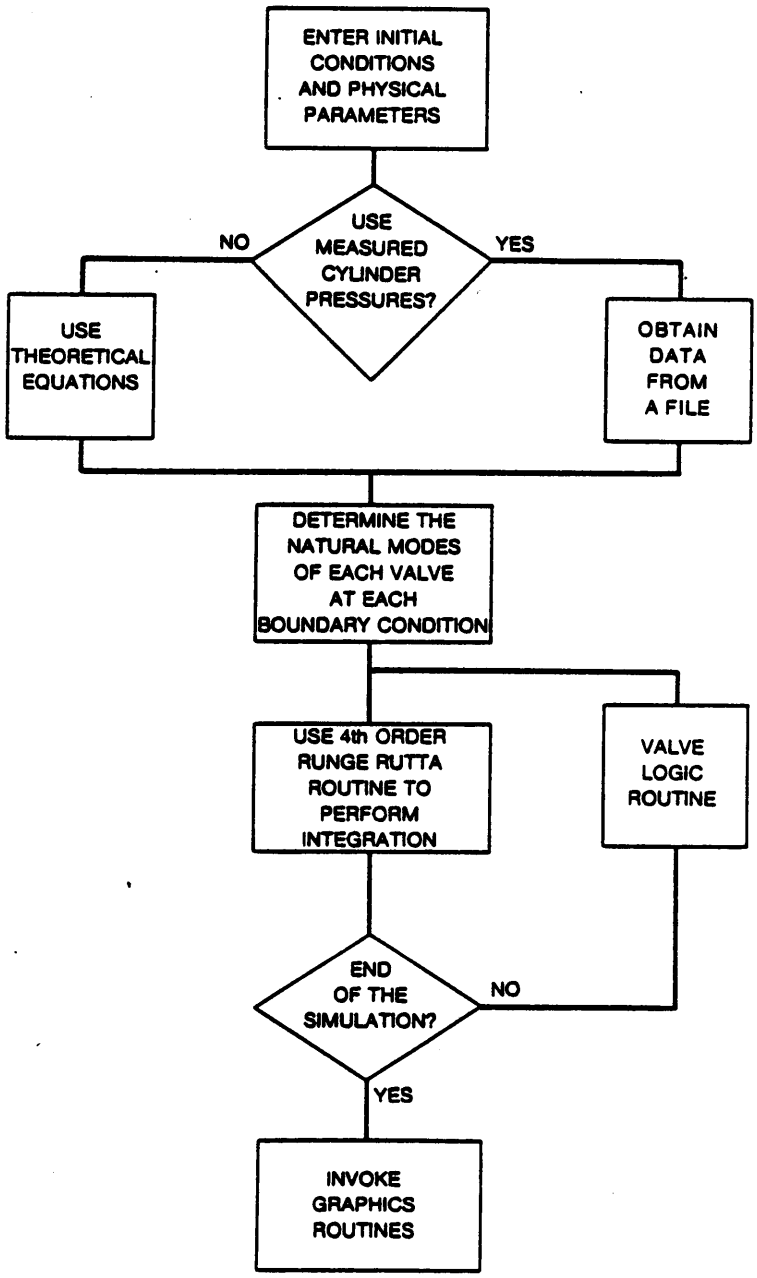

Figure 4.5: Flow chart of the simulation program

3. The exit and entrance flow systems of the cylinder may be modeled as flow through a system of orifices.
4. The intake and exhaust valves are the greatest obstruction to the flow in and out of the cylinder, respectively.
5. The flow changes direction by 90° upon impact with the valve.
6. The valve displacements are small.
7. The torsional modes of the valves contribute little to the valve motion.
8. The transfer matrix method correctly determines the bending natural modes of the valve.
9. The compressor operates at a constant speed

Further assumptions made in the computer program are as follows:

1. Each of the two intake valves and two exhaust valves displace identically.
2. The damping factor, ζ_m, is the same for each natural mode and constant throughout the process. The optimum value being found by experimentation.
3. The polytropic index is constant (varying the polytropic index was found to cause the simulation program to behave unstably). The optimum index was found by experimentation.
4. The flow coefficients, and other factors in the mass flow rate and pressure equations (Eqs. (3.38) and (3.39), respectively) are constant throughout the process. The optimum values were found by experimentation.

5. Since the first stage intake plenum is exposed to the atmosphere, the intake plenum pressure is always equal to the atmospheric pressure.
6. Using the first stage exit plenum pressure takes into account the influence of the second stage on the first.

Another assumption in the simulation program is associated with the nature of the valve stops in the Model 242 compressor shown in Fig. 4.6. As seen the actual valve stops are blocks that start before the tip of the valve. When the valve hits the stop, the valve is constrained at a point before the tip. Therefore, the valve length used in the program is that from the point at which the valve is bolted to the beginning of the valve stop, ℓe in Fig. 4.6. Linear interpolation was used to determine the positions of the valve at points beyond ℓe.

The justification for using the shorter length rests in the fact that the distance from the valve seat to the valve stop is very small: less than or equal to 1.65 mm for all configurations and all valves. Therefore, the valve spends a large part of the cycle time pinned to the stop rather than between the stop and seat.

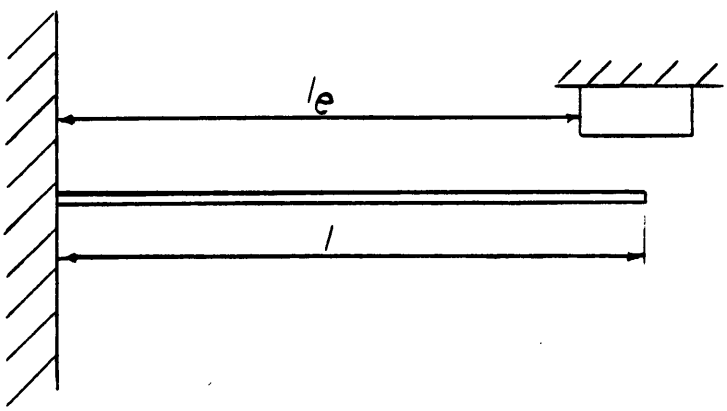

Figure 4.6: The actual valve stop on the Ingersoll Rand Model 242 compressor.

5. RESULTS AND DISCUSSION

In the section to follow the results of the simulation program are compared to the experimental results. The program was run using experimental cylinder pressures at both exhaust valve stop heights, and with the calculated cylinder pressures at only the lower exhaust valve stop heights.

For simplicity, the comparison points on the valves will be referred to as Point 1 and Point 2 as shown in Fig. 4.1 and 4.2 for the intake and exhaust valves, respectively. Also, Case 1 and Case 2 will refer to the smaller and larger exhaust valve stop heights respectively.

5.1 Results Using Measured Cylinder Pressures

As stated earlier, the purpose of using the measured cylinder pressures in the simulation program is to determine deficiencies in the valve dynamics theory free of errors induced by an analytical pressure calculation.

In the analysis of both cases it was found that only three natural modes were necessary to describe the valve motion. The disadvantage of using only three modes is that valve bouncing cannot be predicted. This phenomena will be elaborated on in the discussion of the intake valve results were valve bouncing is evident.

5.1.1 The Exhaust Valve Results

The figures displaying the analytical and experimental comparisons are listed below:

Fig. 5.1) Comparison of the analytical and experimental exhaust valve positions for Case 1, Point 1.

Fig. 5.2) Comparison of the analytical and experimental exhaust valve positions for Case 1, Point 2.

Fig. 5.3) Comparison of the analytical and experimental exhaust valve position for Case 2, Point 1.

Fig. 5.4) Comparison of the analytical and experimental exhaust valve positions for Case 2, Point 2.

An observation made in running the simulation program, which is not evident in the figures, is that the exhaust valve experiences substantial oil stiction. Figures 5.1-5.4 were produced with oil stiction taken into account by increasing the valve preload, P_v, (Eq. 3.39). In Fig. 5.5 the exhaust valve position at Point 1, Case 1 is shown with no increase in the preload. The delay is shown to be approximately 12.5 crank angle degrees, or 2.53 thousands of a second (rotational speed of the crank is 85.9 r/s). Giacommeli, et al. [10] observed oil stiction induced delays of 5 to 20 thousands of a second in their bench test analysis of oil stiction. Also, the effects of oil stiction seem to vary along the length of the valve. This can be observed in both the Case 1 and Case 2 comparisons (Figs. 5.1 and 5.2 and Figs. 5.3 and 5.4, respectively). In both cases increasing P_v has eliminated the effects of oil stiction at Point 1 but not at Point 2.

The comparison of the Case 1 experimental and analytical results at Points 1 and 2 show a reasonable comparison. The largest discrepancy is that the analytical valve stays open approximately 12.5 crank angle degrees. This indicates that theoretical pressure on the valve (Eq. 3.39) overpredicts the pressure on the valve in the latter part of exhaust valve cycle.

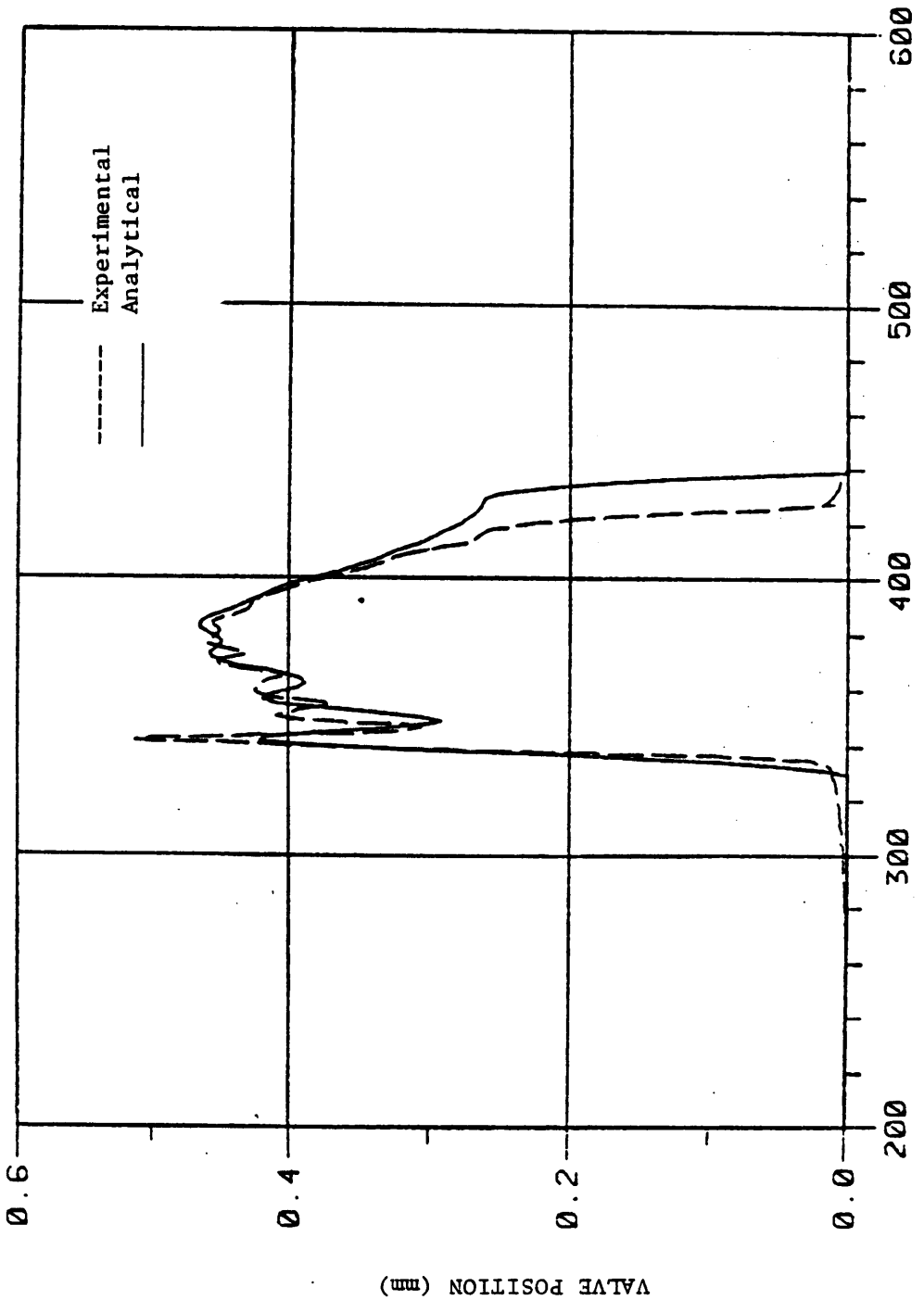

Figure 5.1. The Analytical Exhaust Valve Positions Using Measured Cylinder Pressures Compared to the Experimental Positions for Case 1, Point 1.

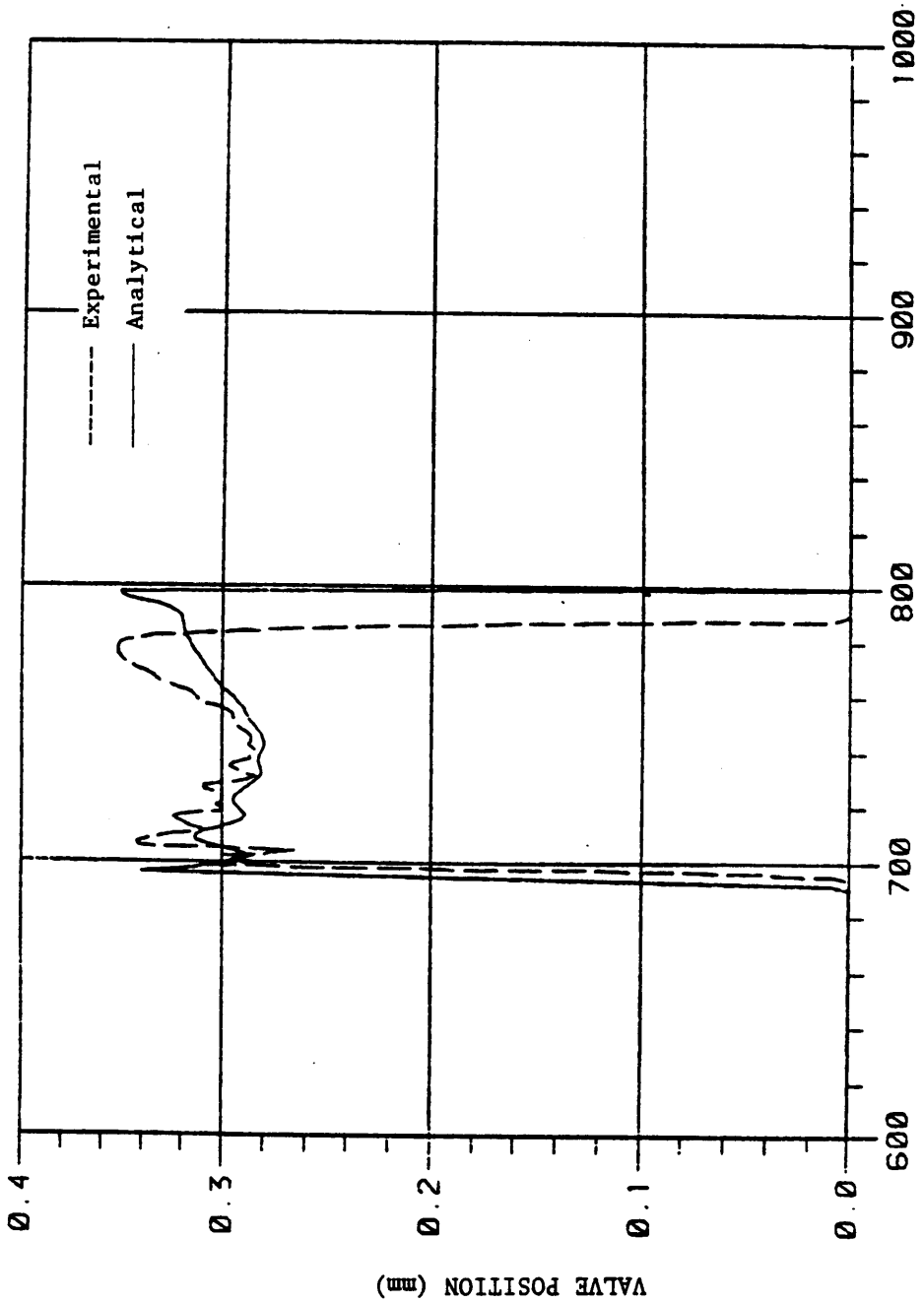

Figure 5.2. The Analytical Exhaust Valve Positions Using Measured Cylinder Pressures Compared to the Experimental Positions for Case 1, Point 2.

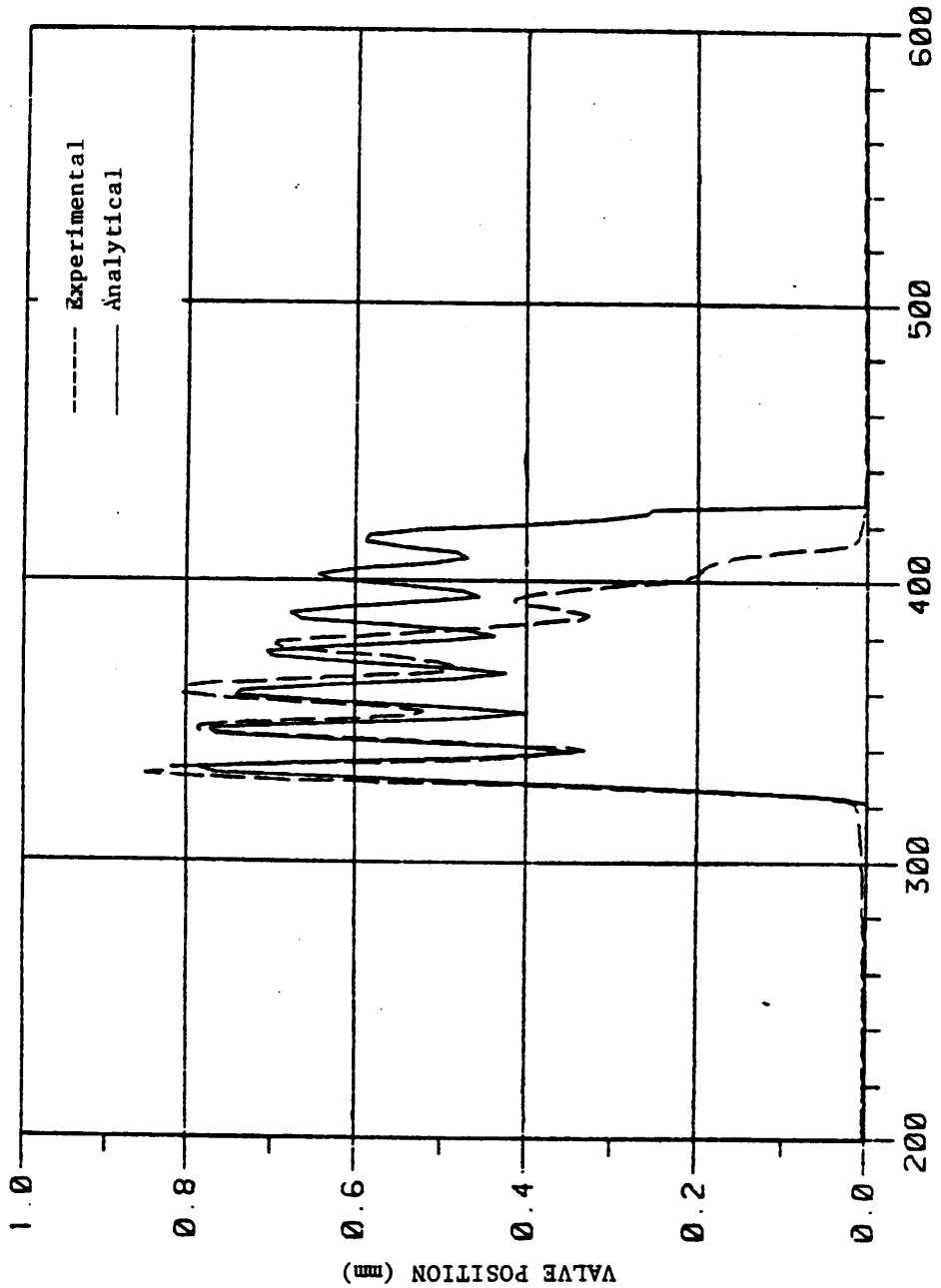

Figure 5.3. The Analytical Exhaust Valve Positions Using Measured Cylinder Pressures Compared to the Experimental Positions for Case 2, Point 1.

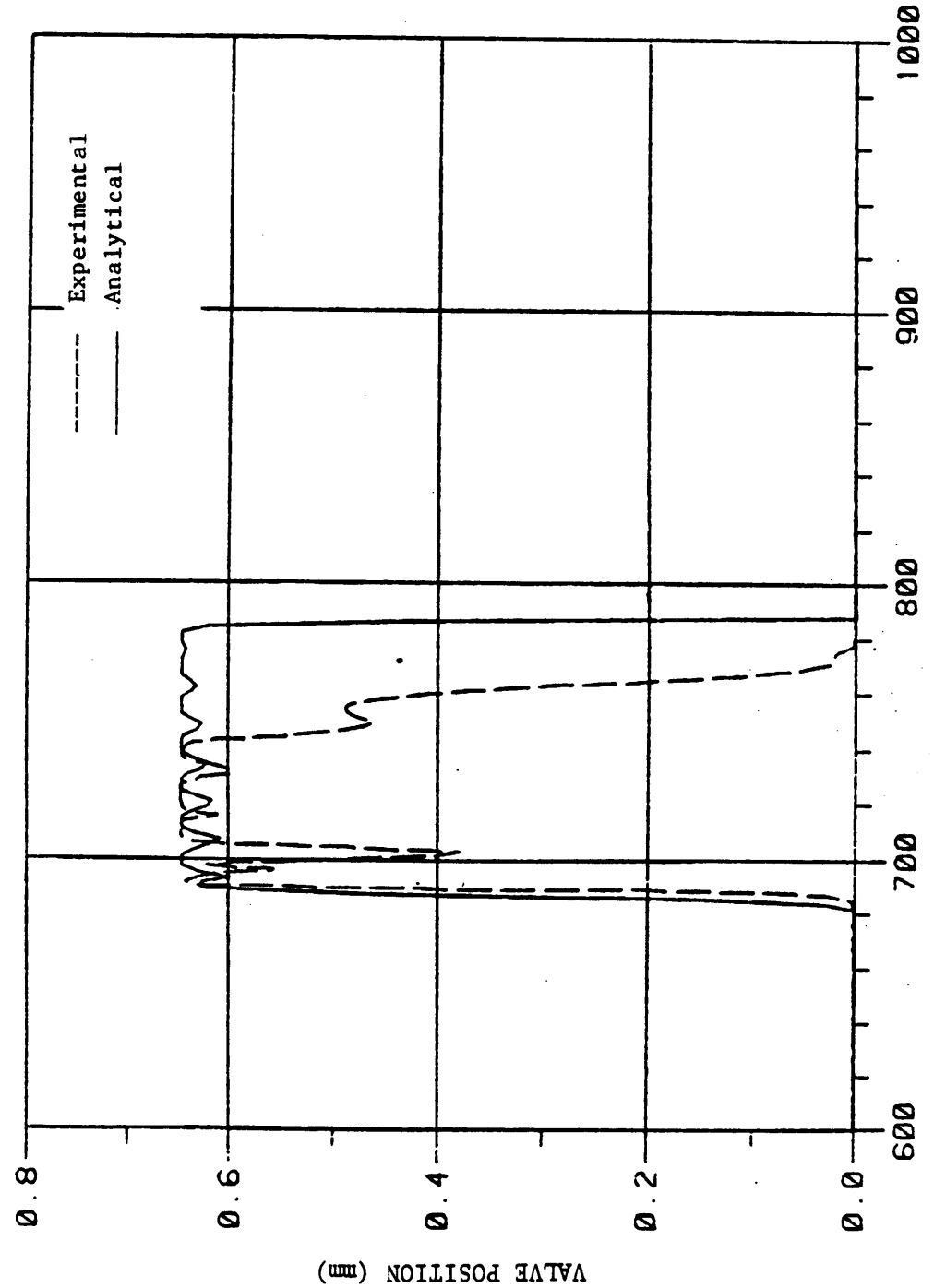

Figure 5.4. The Analytical Exhaust Valve Positions Using Measured Cylinder Pressures Compared to the Experimental Positions for Case 2, Point 2.

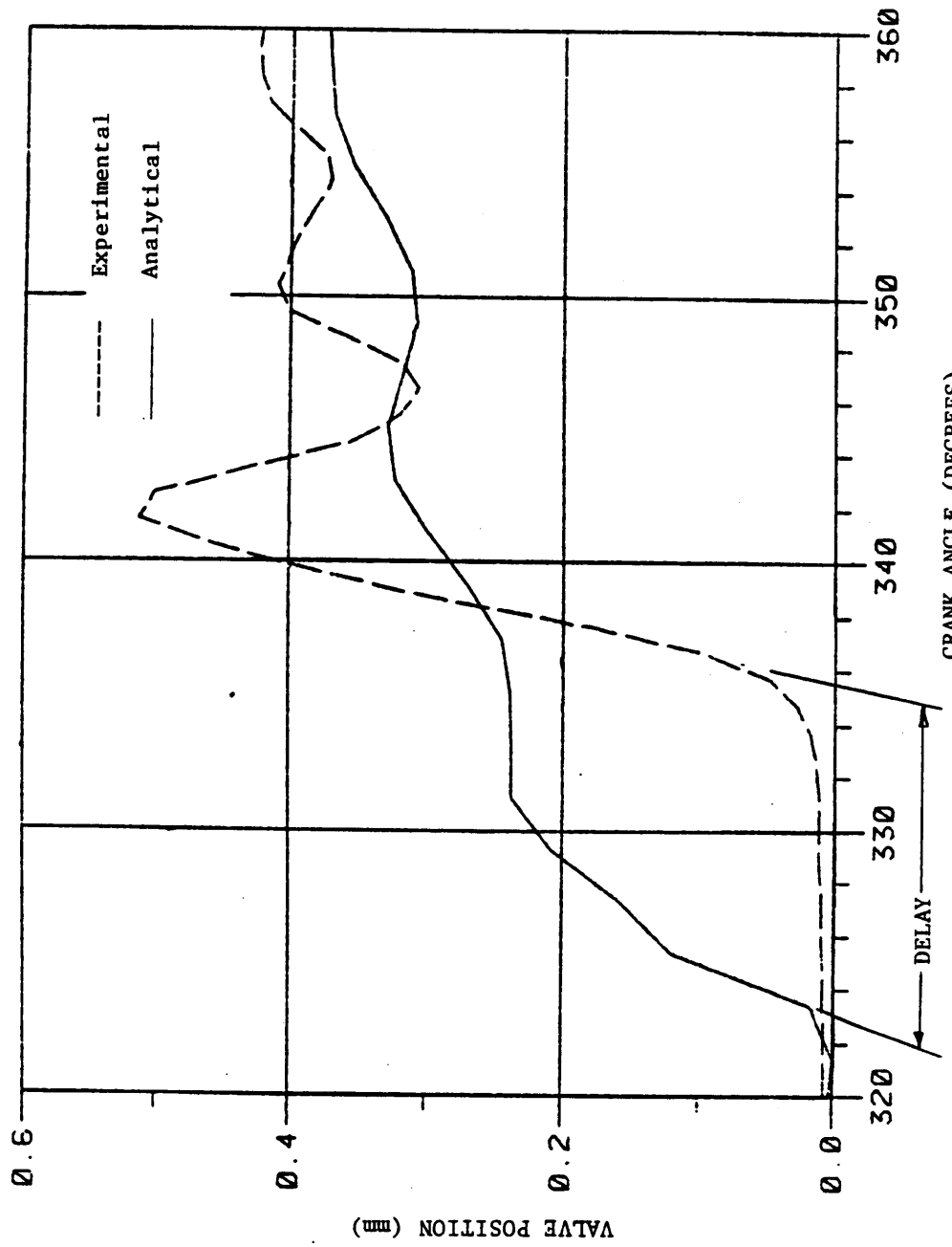

Figure 5.5. Oil Stiction Induced Delay of the Exhaust Valve at Point 1, Case 1.

In the Case 2 comparisons at Point 1 and 2, the discrepancy in the latter part of the valve cycle is much greater than the discrepancy seen in Case 1. At both Points 1 and 2 in Case 2 the actual valve displacement begins to drop off much earlier than the analytical model predicts. Before the start of the discrepancy in Case 2, however, the comparison in the analytical and experimental results is very good.

In Figure 5.6 the calculated pressure on the valve is compared to the actual valve position for Case 2, Point 1. As seen the calculated pressure holds relatively constant when the valve is actually starting to close. Since the pressure on the valve calculation is mainly based on steady flow through the valves, it is hypothesized that there is an unsteady flow phenomena that causes the pressure to drop and the valve to close. One explanation for this unsteady flow phenomena is the second stage flow dynamics are adversely affecting the first stage flow dynamics. Since the first stage exit plenum is connected to the second stage inlet plenum by pipe work, closure of the second stage intake valve can cause the flow between the stages to stagnate. Therefore, due to the stagnation of the flow, flow forces develop on the exhaust valve which may cause the first stage exhaust valve to close.

Another interesting observation is that the valve damping decreases with increasing valve stop height. This is seen by comparing the Case 1 (lower stop height) and Case 2 (higher stop height) experimental results at Point 1. As seen the valve in the Case 2 configuration is visibly less damped. Since a lightly damped valve undergoes more fatigue cycles in a given time period, this suggests a lower stop height increases the fatigue life of finger valves.

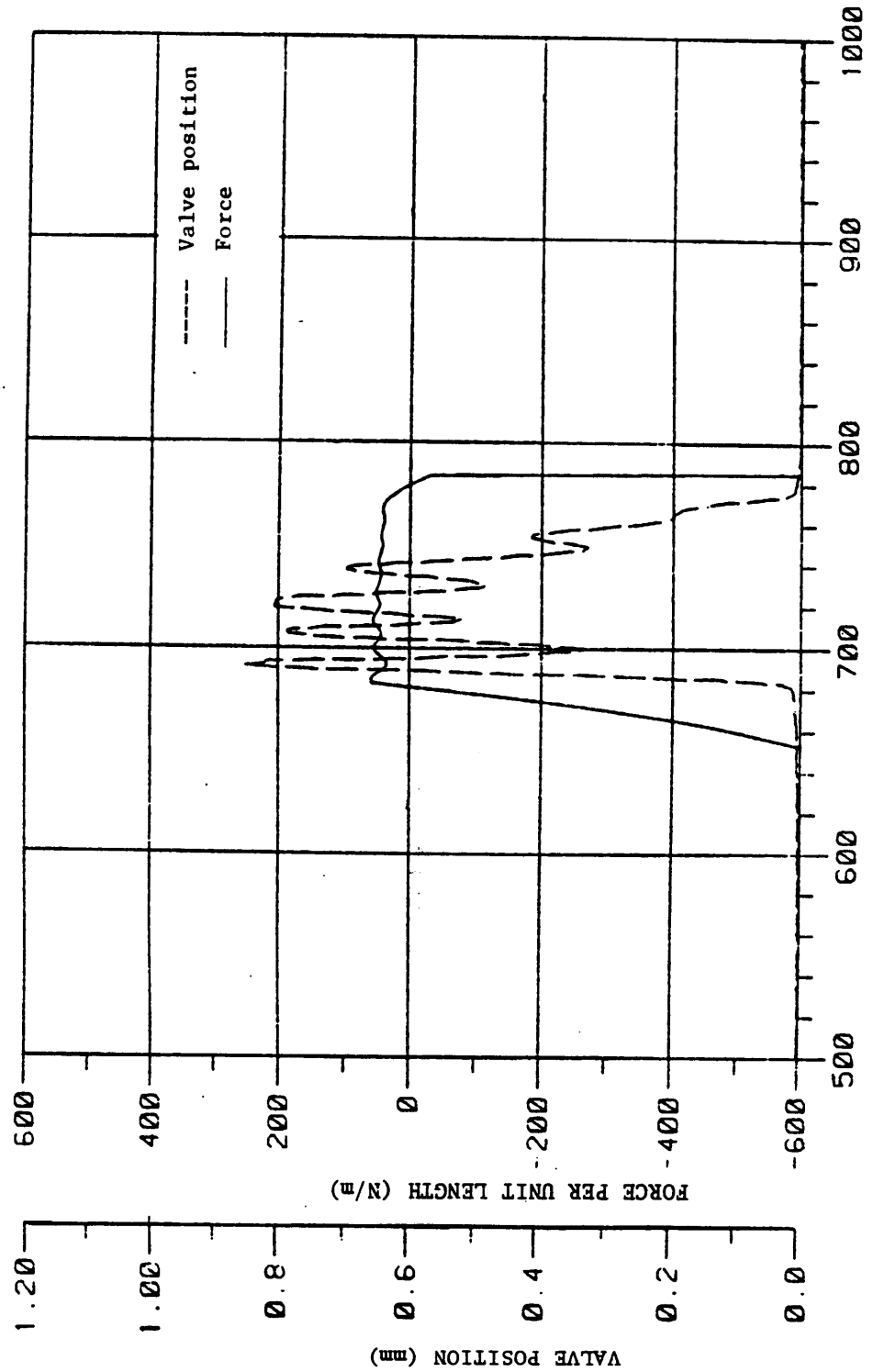

Figure 5.6. Experimental Exhaust Valve Positions at Point 1, Case 2 Compared to the Calculated Force Per Unit Length on the Valve.

5.1.2 Intake Valve Results

As stated earlier, due to experimental limitations the intake valve position could not be measured in the increased exhaust valve stop configuration (Case 2), so only Case 1 comparisons will be made in this section. The comparisons are shown in Figs. 5.7 and 5.8 for Points 1 and 2, respectively.

The results in Figs. 5.7 and 5.8 show that the analytical intake valve stays open much longer than the actual valve. In Fig. 5.9 the piston velocity is plotted along with the actual intake valve displacement at Point 2. As seen, the actual valve closes very quickly after the piston reverses direction. Therefore, it is theorized that reversal of the piston induces a flow force on the valve that is not predicted by the theory.

Applying a large force to the analytical intake valve after the piston reverses direction, the positions for Points 1 and 2 are shown in Fig. 5.10 and 5.11, respectively. As seen the analytical intake valve closure, although more abrupt than the actual valve, now occurs at approximately the same time as the actual intake valve. However, the analytical valve stays at too high of a level before closure.

In order to further improve the correlation the following relation was used:

$$\overline{P}(t) = Q_B \, \dot{X}(t)^2 \, P(t) \tag{5.1}$$

where

$\overline{P}(t)$ = corrected pressure on the valve

$\dot{X}(t)$ = piston velocity

$P(t)$ = uncorrected pressure on the valve (Eq. 3.39)

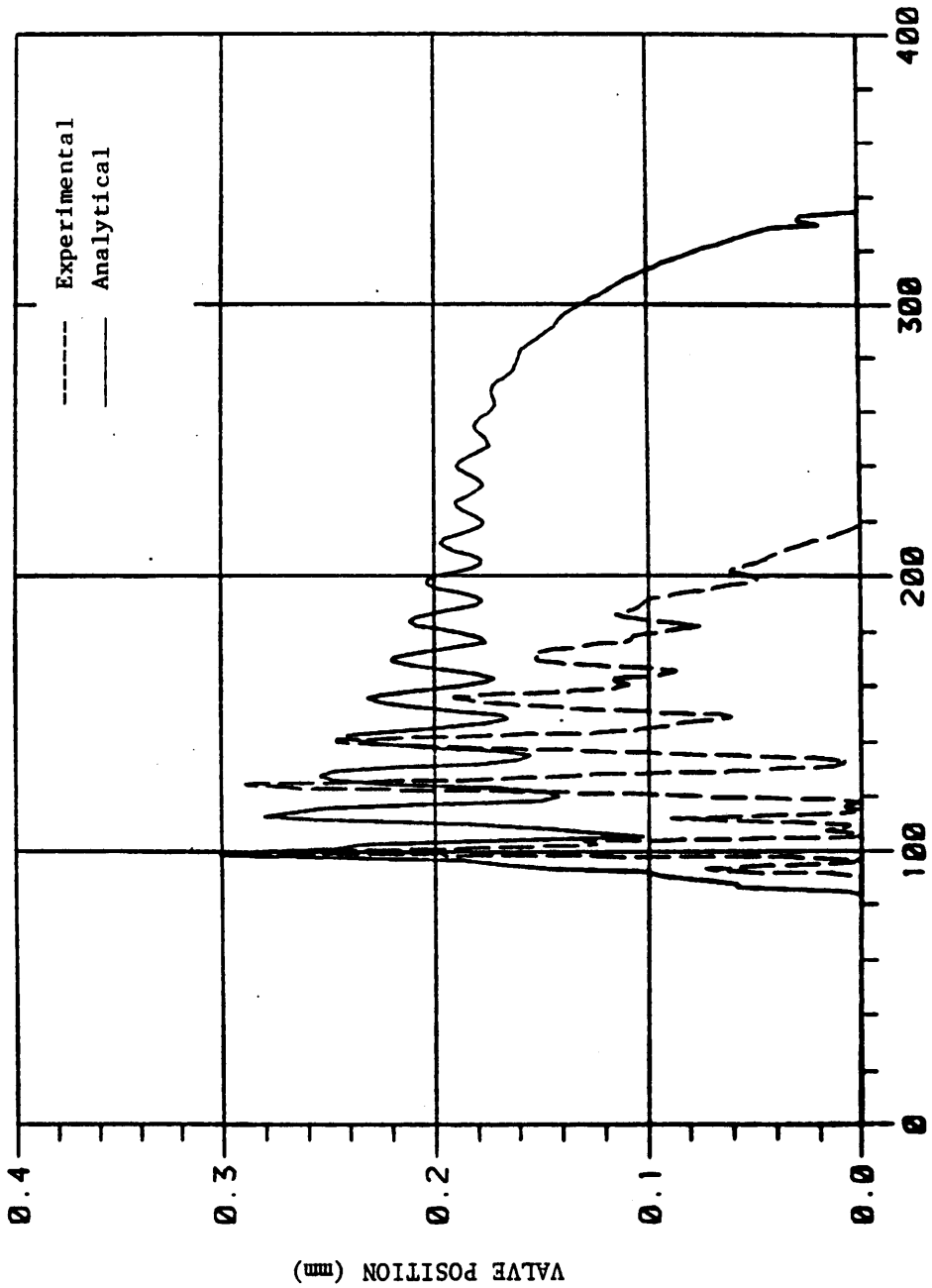

Figure 5.7. The Analytical Intake Valve Positions Using Measured Cylinder Pressures Compared to the Experimental Positions at Point 1.

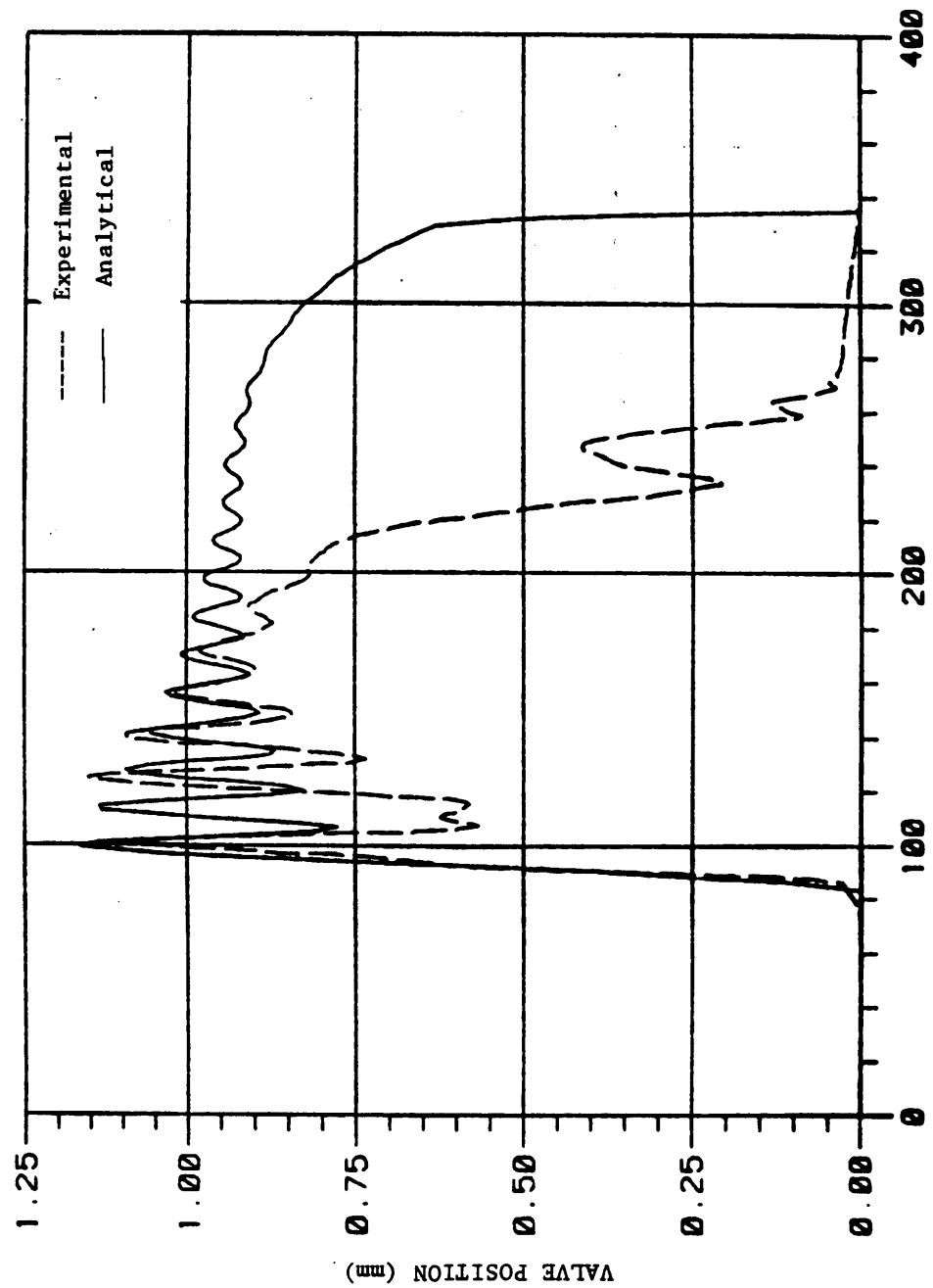

Figure 5.8. The Analytical Intake Valve Positions Using Measured Cylinder Pressures Compared to the Experimental Positions at Point 2.

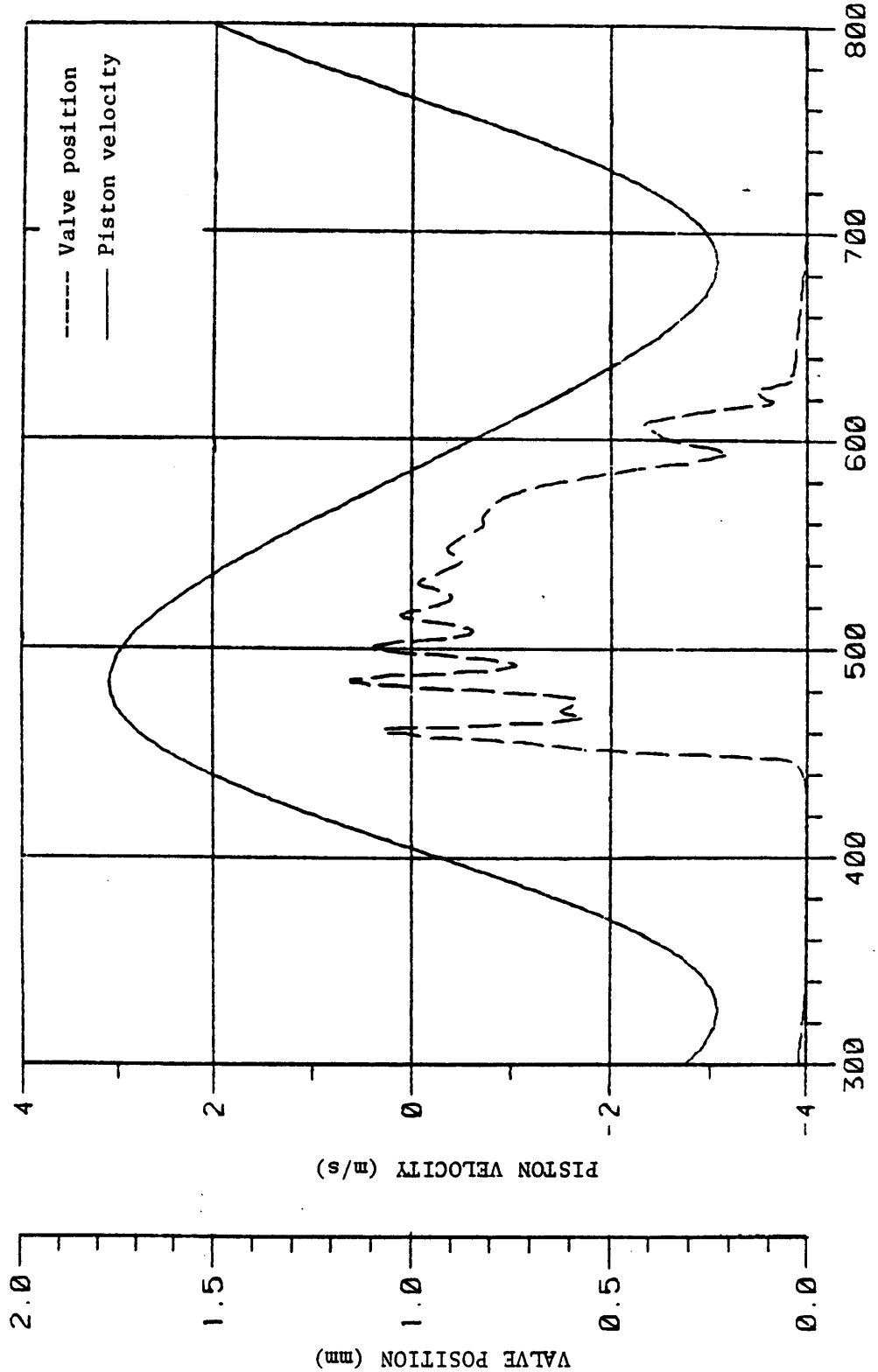

Figure 5.9. The Experimental Intake Valve Positions at Point 1 Compared to the Piston Velocity.

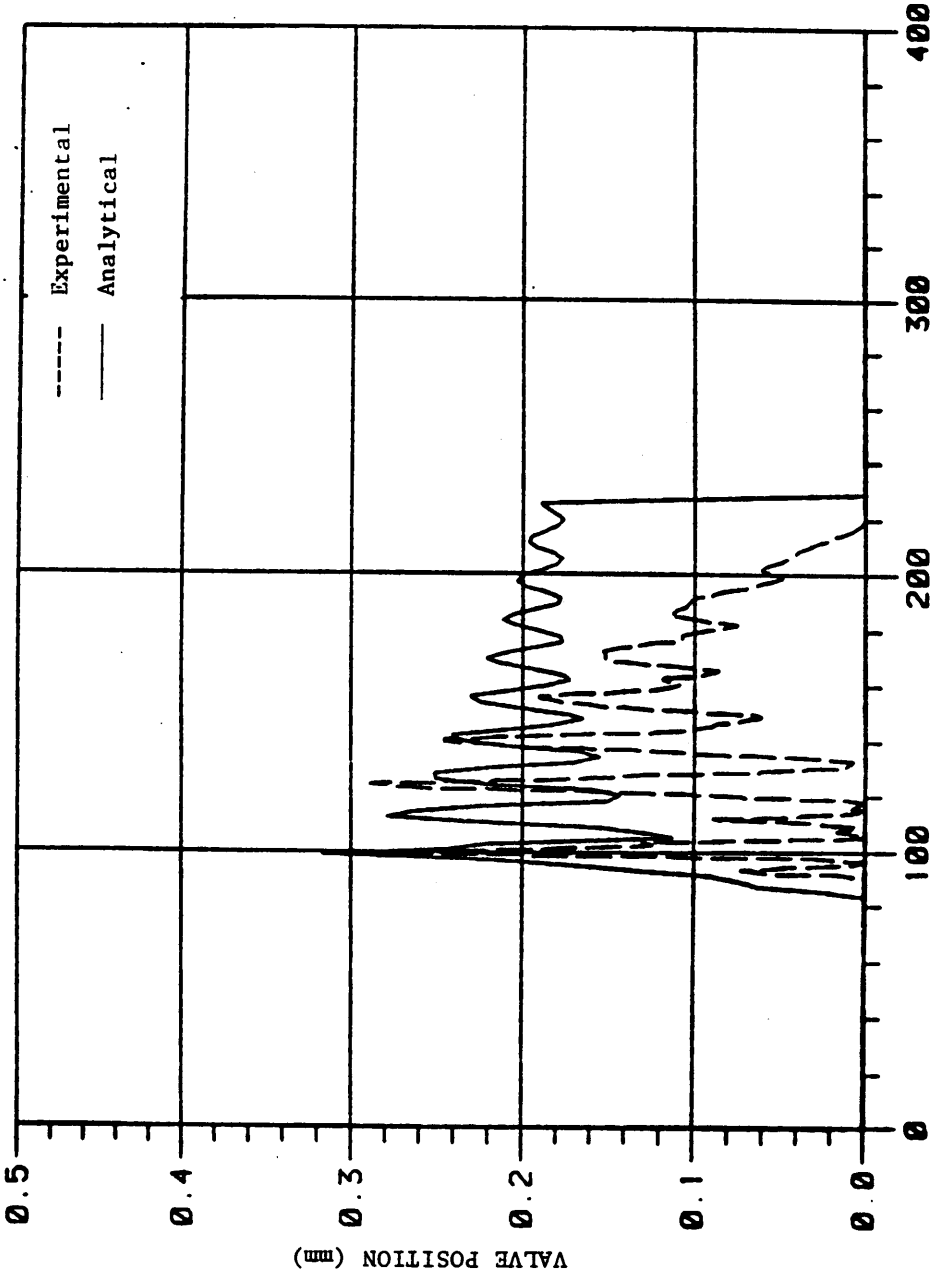

Figure 5.10. Comparison of the Analytical and Experimental Intake Valve Positions at Point 1 when the Analytical Valve is Forced to Close at Piston Reversal.

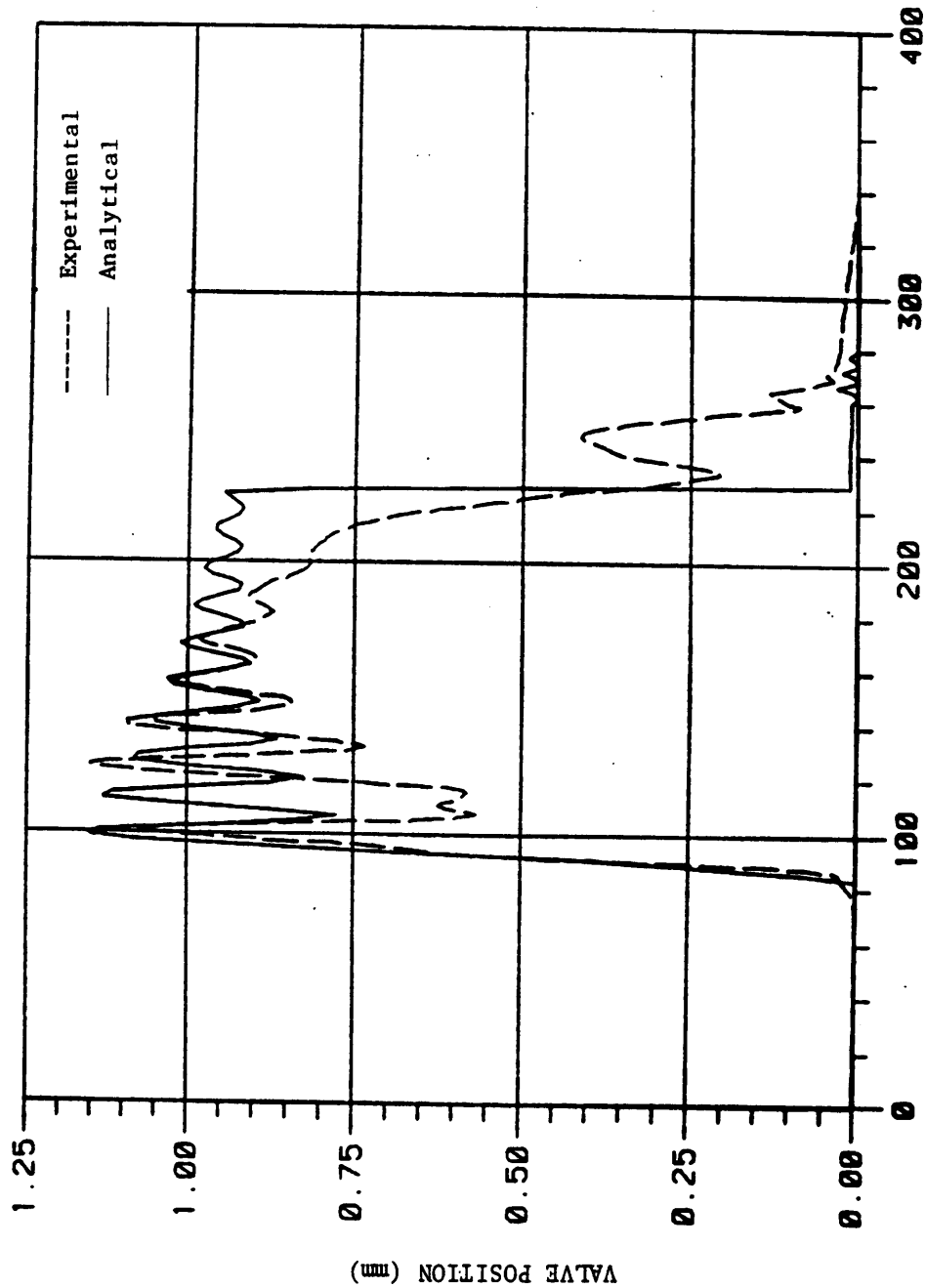

Figure 5.11. Comparison of the Analytical and Experimental Intake Valve Positions at Point 2 when the Analytical Valve is Forced to Close at Piston Reversal.

Equation 5.1 is not meant to depict a physical relation but instead to be a means of varying the flow coefficients in Eq. (3.39) which are otherwise assumed to be constant.

The combined effects of applying a large force on the valves and using Eq. 5.1 are seen in Figs. 5.12 and 5.13 for Points 1 and 2, respectively. As seen the general trend of the motion is now predicted well, but the large oscillations in motion are still not predicted. These oscillations in the motion are hypothesized to be due to oscillations in the flow.

An important observation to make about Fig. 5.13 is that the peaks that occur at the end of the actual valves cycle are not predicted by the analytical model. These peaks are assumed to be the valve bouncing on the seat as the valve closes.

As mentioned earlier, the valve positions are described with only the first three natural nodes. When valve bouncing occurs it was found that three modes are insufficient to correctly describe the motion. In fact, the truncated set of modes yielded extraneous results. So, bounce analysis, as presented in Chapter 3, requires the higher modes. However, extending the model to just 5 modes provided no improvement to the results while making the program computationally slow.

Also, the intake valve was found to experience no effects of oil stiction. It is theorized that since the intake port brings in air from the atmosphere, the air contains no oil and, therefore oil is not deposited on the valve and its seat eliminating any delay due to oil stiction. On the other hand, the exhaust valve experiences the effects of oil stiction since the valve is exposed to air with a significant oil

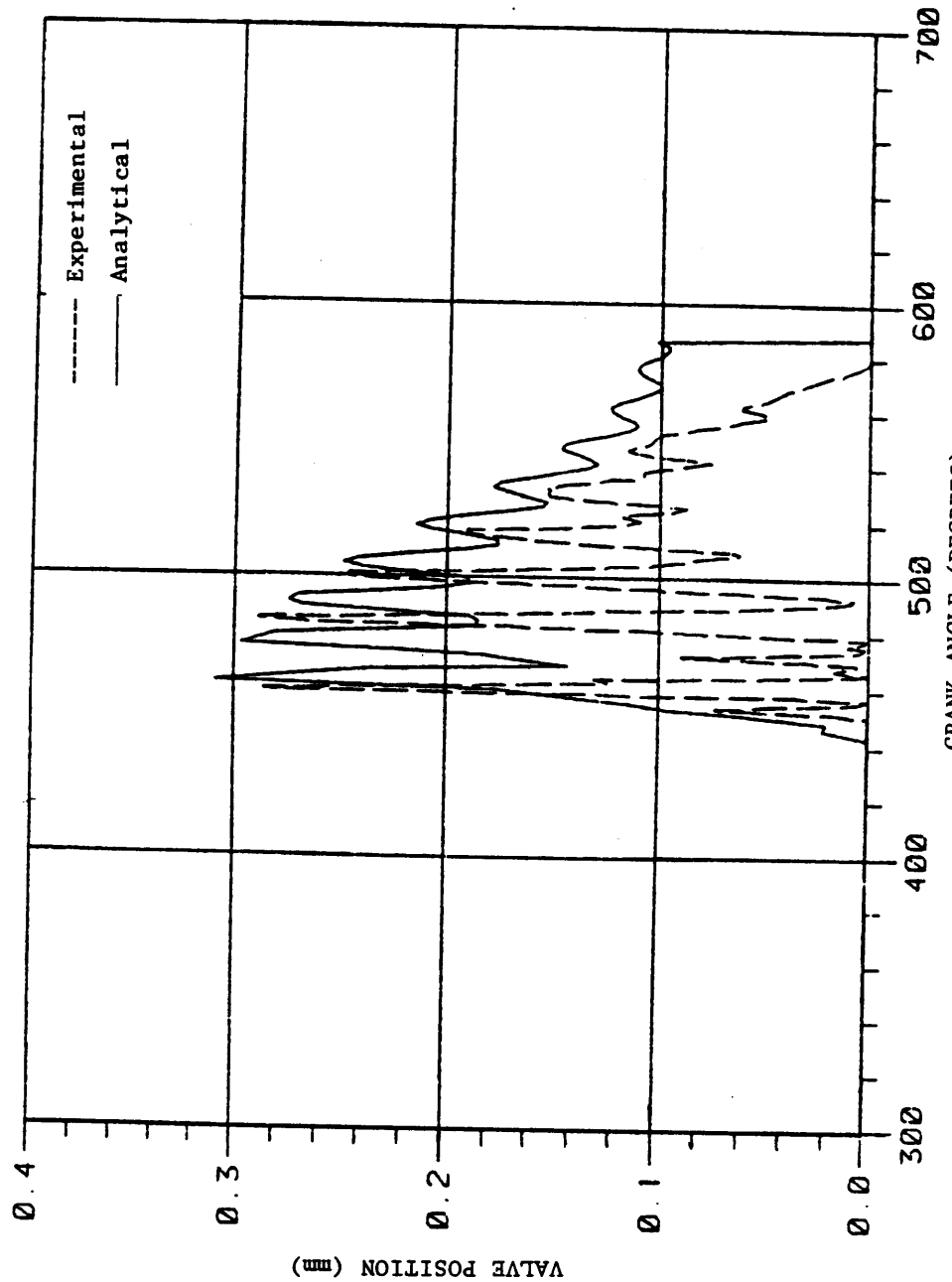

Figure 5.12. Comparison of the Analytical and Experimental Intake Valve Positions at Point 1 when the Analytical Valve is Forced to Close at Piston Reversal and the Flow Coefficients are Varied.

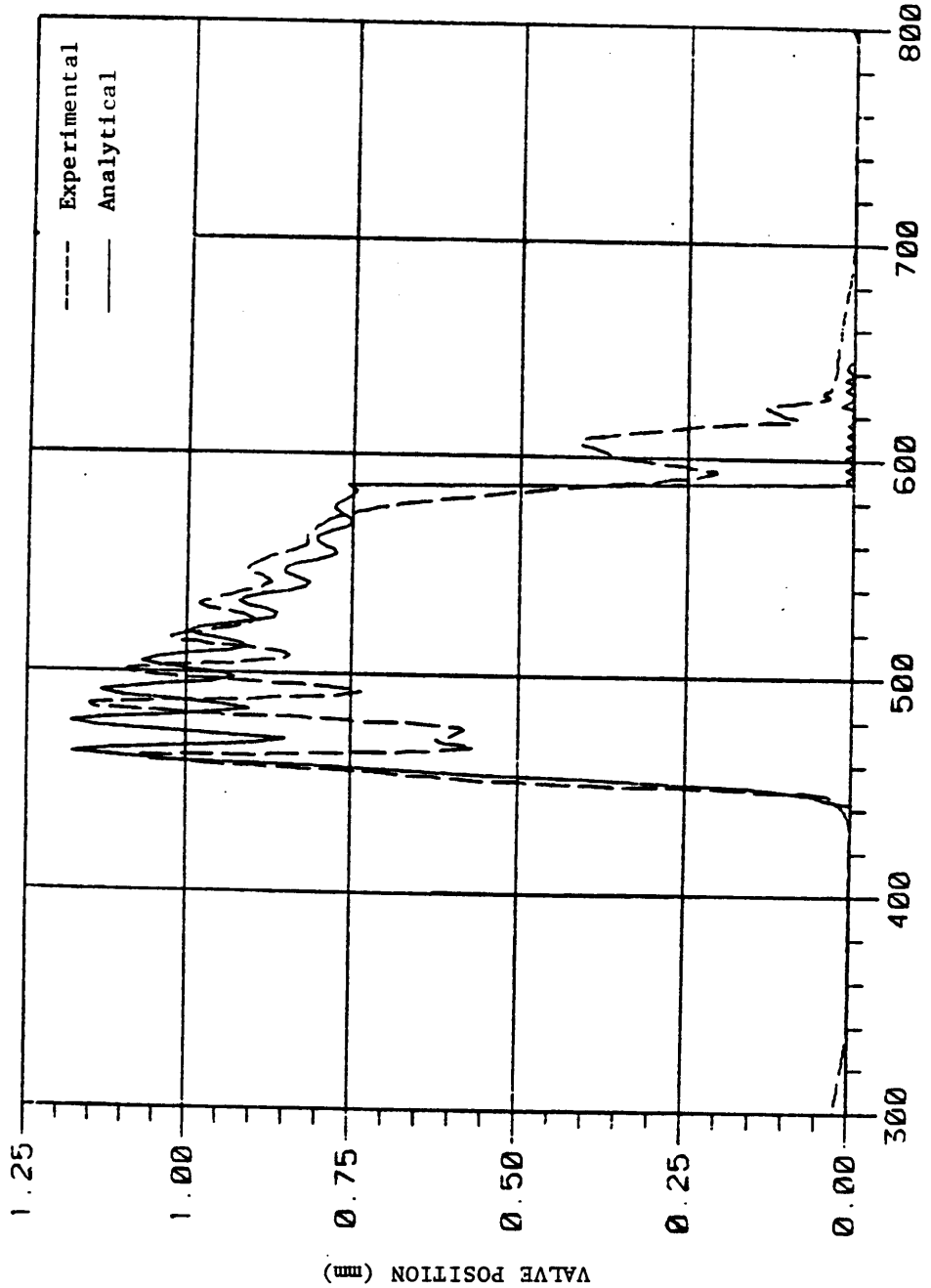

Figure 5.13. Comparison of the Analytical and Experimental Intake Valve Positions at Point 2 when the Analytical Valve is Forced to Close at Piston Reversal and the Flow Coefficients are Varied.

content. The air that exits the exhaust port obtains oil while it is in the cylinder cavity. Oil is scraped off the cylinder walls by the piston motion and partially carried away by the air.

5.2 Results Using Calculated Cylinder Pressures

In the analysis using calculated pressures, the analysis used the same coefficients and factors that were used in the analysis using measured pressures. Also, this analysis used the adjustments in the force on the intake valve used to produce Figs. 5.12 and 5.13. The justification in doing so was to reproduce the intake valve position in order to minimize the errors introduced into the thermodynamic and fluid mechanics equations.

Also, only three modes were found necessary to reproduce the valve motion.

Due to the fact that the intake valve position could not be measured at the higher exhaust valve stop height (Case 2), the analytical analysis using calculated cylinder pressures was performed only in the Case 1 configuration.

The figures comparing the analytical results to the actual results are listed below:

Fig. 5.14) Cylinder pressure comparison

Fig. 5.15) Comparison of intake valve positions at Point 1

Fig. 5.16) Comparison of intake valve positions at Point 2

Fig. 5.17) Comparison of exhaust valve positions at Point 1

Fig. 5.18) Comparison of exhaust valve positions at Point 2

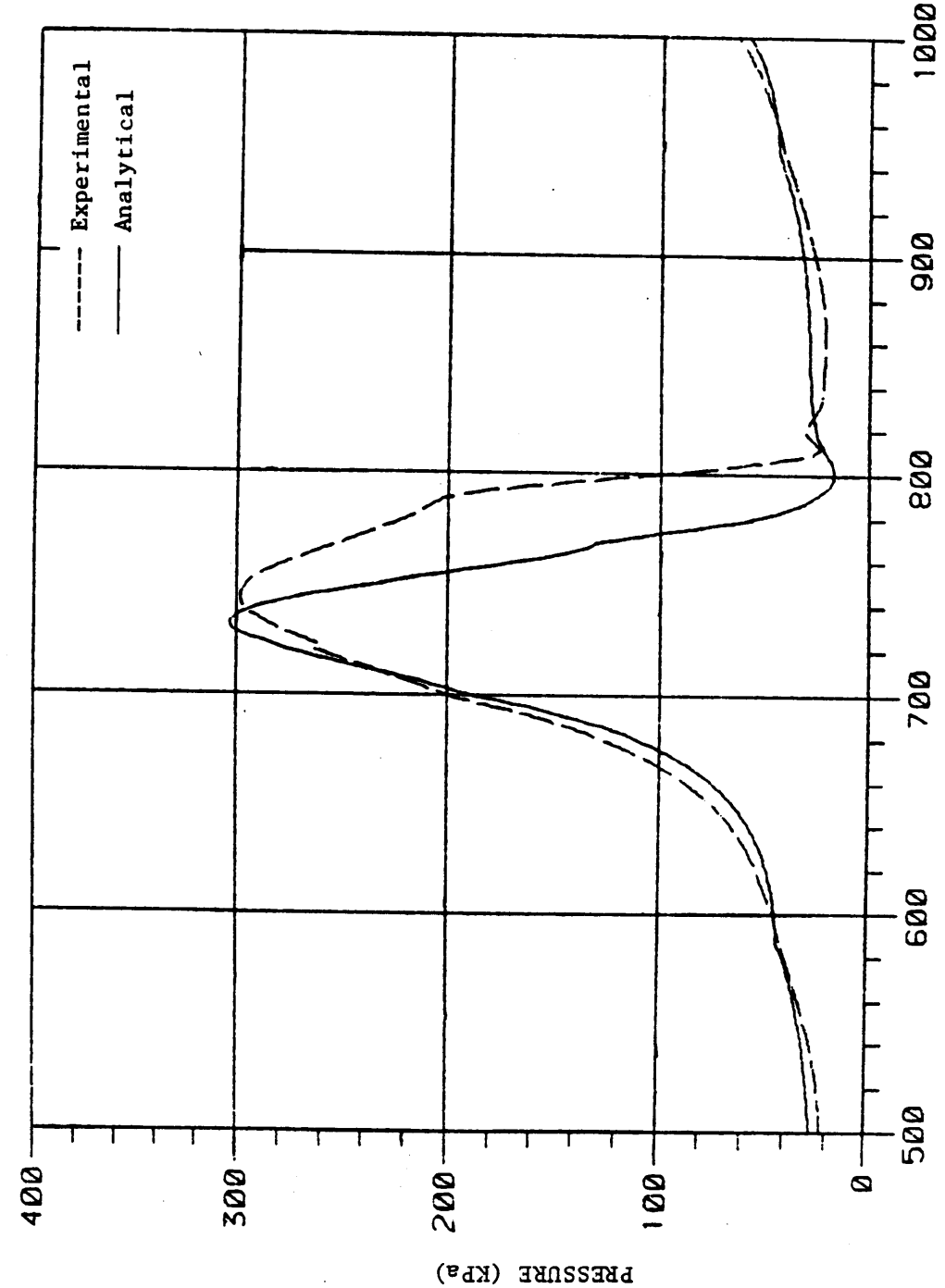

Figure 5.14. Comparison of the Calculated and Experimentally Measured Cylinder Pressures.

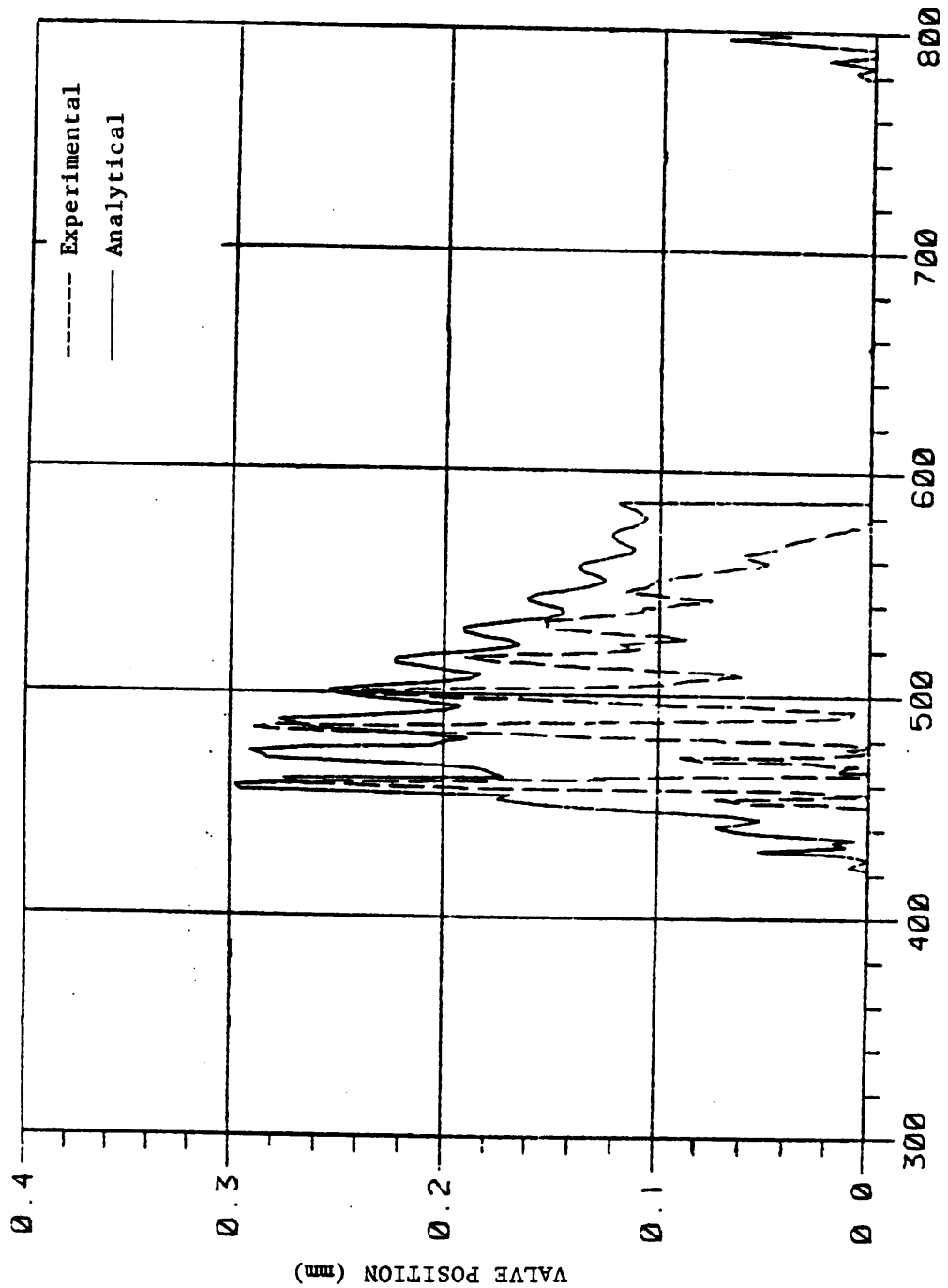

Figure 5.15. The Analytical Intake Valve Positions Using Calculated Cylinder Pressures Compared to the Experimental Positions at Point 1.

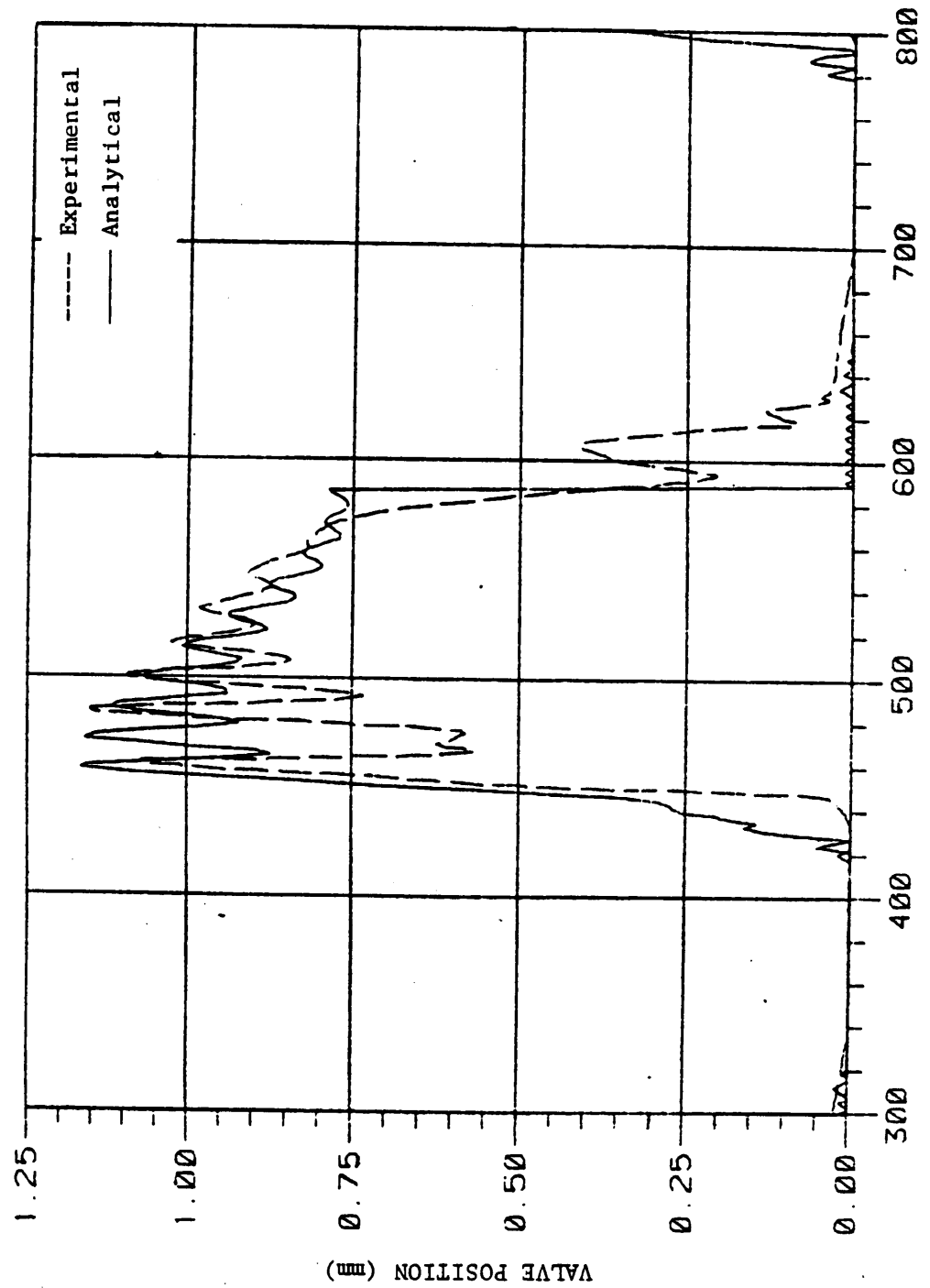

Figure. 5.16. The Analytical Valve Positions Using Calculated Cylinder Pressures Compared to the Experimental Positions at Point 2.

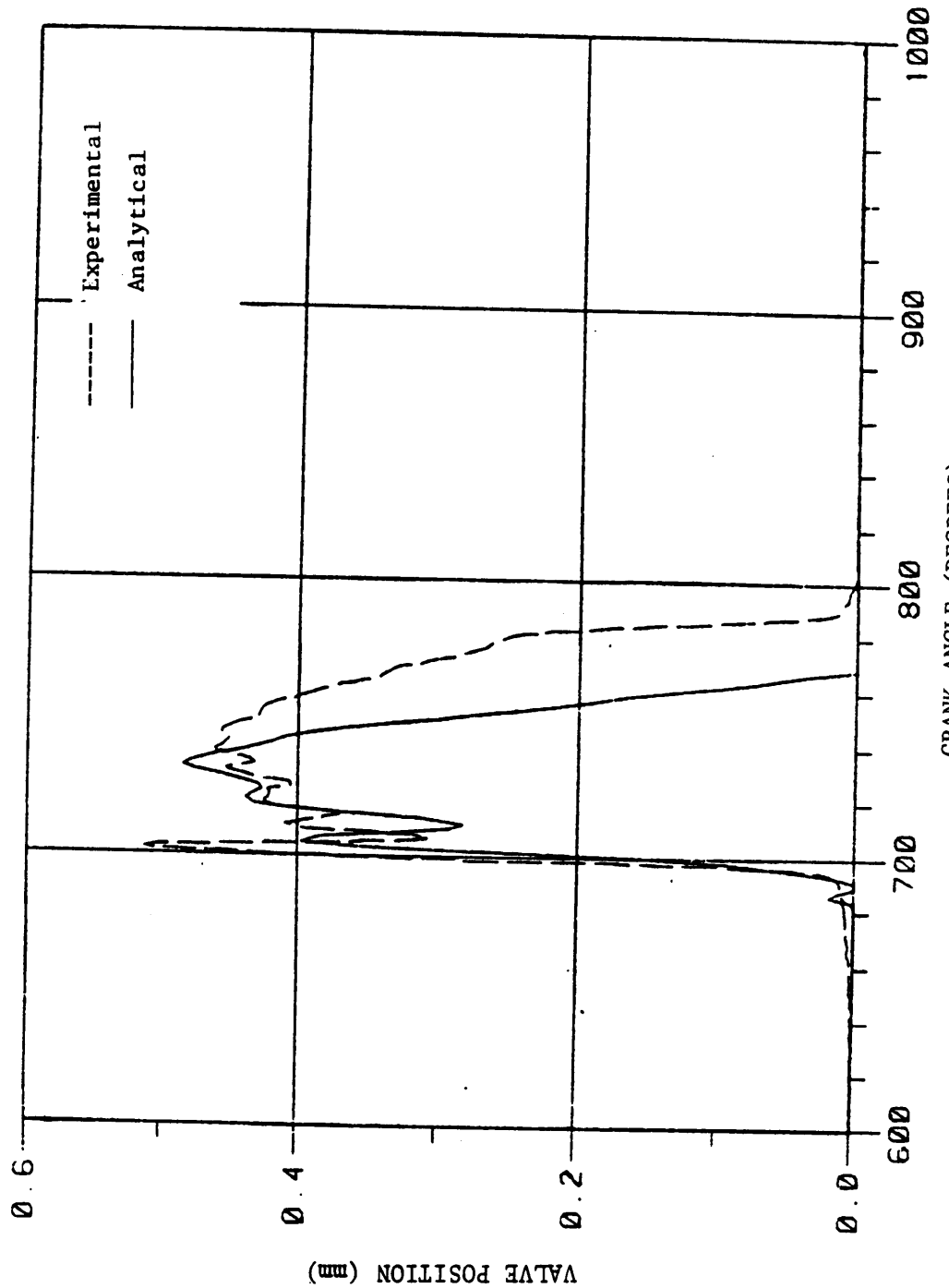

Figure 5.17. The Analytical Exhaust Valve Positions Using Calculated Cylinder Pressures Compared to the Experimental Positions at Point 1.

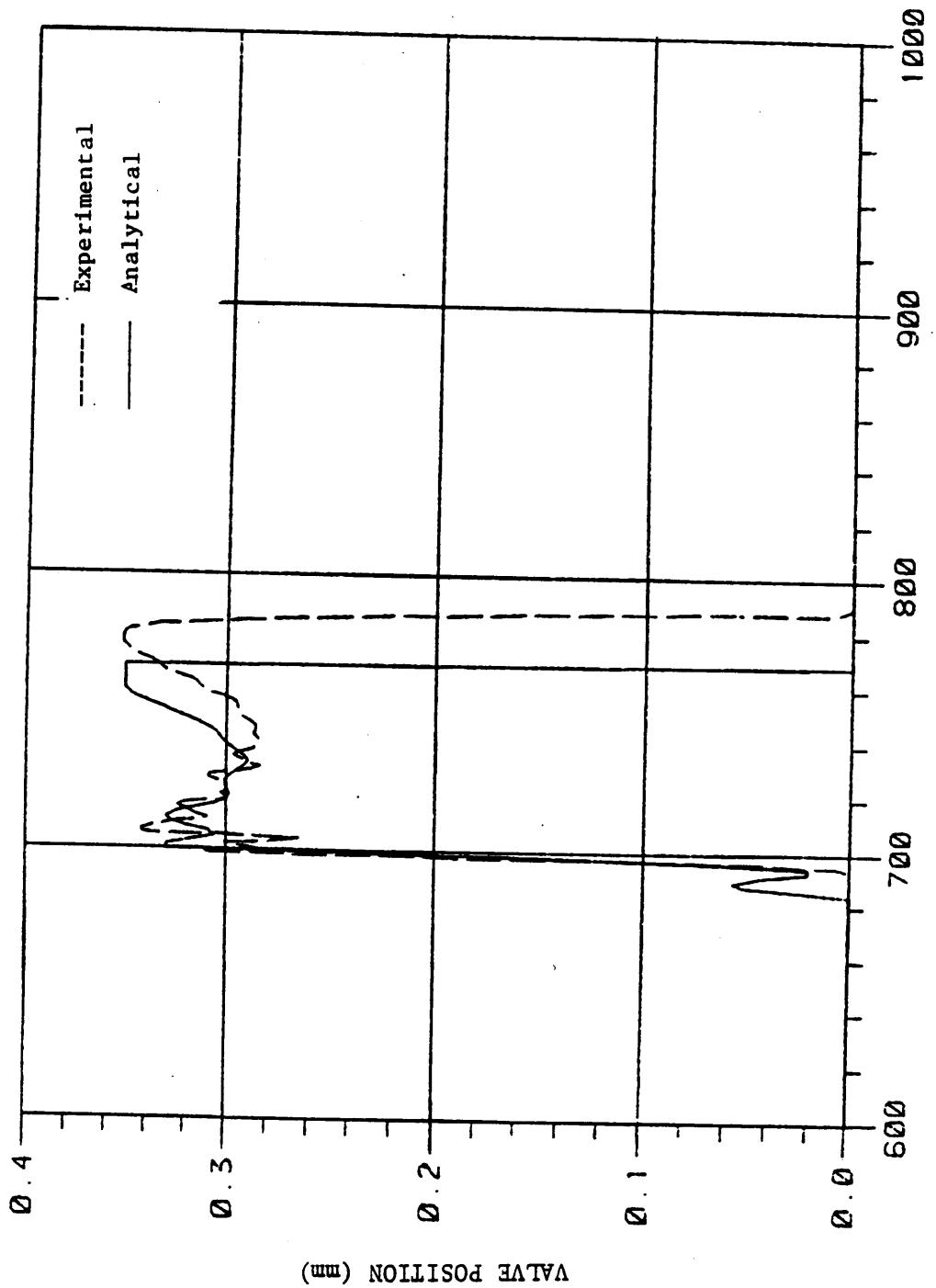

Figure 5.18. The Analytical Exhaust Valve Positions Using Calculated Cylinder Pressures Compared to the Experimental Positions at Point 2.

Figures 5.15 and 5.16 show that the analytical intake valve position predictions are comparable to the predictions shown in Figs. 5.12 and 5.13, which were produced using measured cylinder pressures. Figs. 5.17 and 5.18, the exhaust valve comparisons, show that the model predicts premature closure of the exhaust valve.

This premature closure of the exhaust valve is due to the poor correlation between the analytical and experimental curves during the expansion part of the compression process (Fig. 5.14). As stated earlier, the compression process is assumed to be polytropic. Therefore, the plot of logarithm of the actual cylinder pressure versus the logarithm of the actual cylinder volume (Fig. 5.19) should have a straight line relationship as originally shown in Fig. 3.11. As seen in Fig. 5.19, the slope varies. However, Fig. 5.19 shows the combined effects of the thermodynamic and fluid mechanic processes. So, a varying slope could be due totally to the fluid processes. Determination of the correct method to model the thermodynamic process, therefore, requires an extensive experimental analysis of the fluid as well as the thermodynamic processes that occurs inside the cylinder volume.

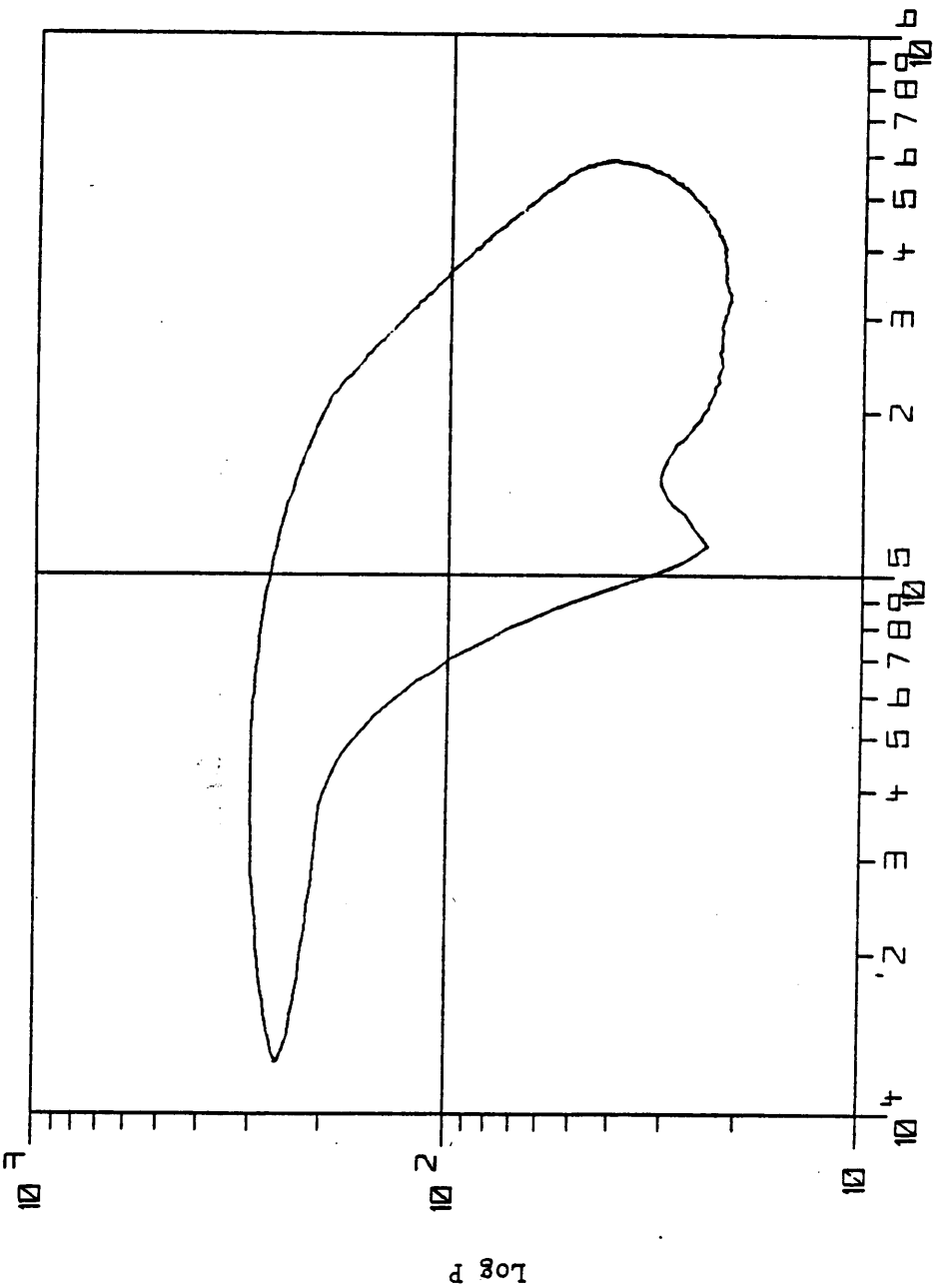

Figure 5.19. Log P vs. Log V Plot of the Model 242 Compressor

6.0 CONCLUSIONS AND RECOMMENDATIONS

In the sections to follow, the conclusions will be drawn from the comparisons of the analytical model with the actual compressor. Based on these conclusions, recommendations for further research will be made.

6.1 Conclusions

In the previous chapters a theoretical compressor model was presented. Results of the computer implementation of the theory were compared to data from an Ingersoll Rand Model 242 compressor. The positive conclusions that can be drawn from the comparisons are as follows:

1. The use of plate theory to describe the valve motion is effective.
2. The use of the transfer matrix method is an efficient method to determine the valves natural modes.
3. The equivalent viscous damping usee to model the valve damping appears valid.
4. The model predicts the exhaust valve motion for a small valve stop height with reasonable accuracy.
5. Valve damping tends to decrease with increasing valve stop height.
6. The effect of oil stiction is evident in the operation of the exhaust valve.
7. Although not substantiated, the effects of oil stiction vary along the length of the valve.
8. Only three modes are necessary to describe the displacement of the valve under most of its elastic configurations.

An area of considerable discrepancy is the determination of the forces on the valve. In all cases there were unexplained oscillations in the valve motion. The theory assumes steady flow through the valve. Therefore, the unexplained oscillations are either due to unsteady flow or other unexplained flow forces or a combination of both.

The determination of the oscillations in the valve motion may have a direct parallel to the areas of poor correlation between the analytical and calculated cylinder pressure curves. Both the valve motion and the cylinder pressure depend heavily on the mass flow rate calculation.

Although there were definite discrepancies found in the simplified compressor model, there was a significant amount of correlation to justify further research.

6.2 Recommendations

The recommendations for further research are as follows:

1) Experimentally study the flow dynamics of the compressor.
2) Experimentally study the thermodynamic process that occurs in the compressor.
3) Inclusion of the second stage of the compressor in the analytical mode or use of a single stage compressor.
4) Analytical investigation of the proper modeling of bounce analysis.

REFERENCES

1. Costagliola, M., "The Theory of Spring Loaded Valves for Reciprocating Compressors," Journal of Applied Mechanics, 17, #4, (1950), p. 415.

2. MacLaren, J. F. T., and S. V. Kerr, "An Analytical and Experimental Study of Self-Acting Valves in a Reciprocating Air Compressor," Proceedings of the International Mechanical Engineering Conference; Industrial Reciprocating and Rotary Compressors, Paper No. 3, London, 1970.

3. Wambsgnass, M. W., and Cohen, R., "Dynamics of a Reciprocating Compressor with Automatic Reed Valves, Proceedings of the XII International Congress on Refrigeration, Paper No. 3.06, Madrid, 1967.

4. Soedel, W., Introduction to Computer Simulation of Positive Displacement Compressor: A short Course Text, Ray W. Herrick Laboratories, Purdue University, 1972.

5. Hamilton, J. F., Extensions of Mathematical Modeling of Positive Displacement Type Compressors, Ray W. Herrick Laboratories, Purdue University, 1975.

6. Gatecliff, G. W., and E. R. Lady, "Forced Vibration of a Cantilever Valve of Uniform Thickness and Non-uniform Width," Proceedings of the 1972 Purdue Compressor Technology Conference, Purdue Research Foundation, 1972.

7. Papastegious, S., Brown, J., and MacLaren, J. F. T., "The Dynamic Behavior of Valve Reeds in Reciprocating Gas Compressors," Proceedings of the 1980 Purde Technology Conference, Purdue Research Foundation, 1980.

8. Gatecliff, G. W., Criner, G. C., and Richardson, H., "A Compressor Valve Model for Everyday Use," Proceedings of the 1980 Compressor Technology Conference, Purdue Research Foundation, 1980.

9. Richardson, H., Gatecliff, G. W., and Griner, G. C., "Verification of Flapper Suction Valve Simulation Program," Proceedings of the 1980 Purdue Compressor Technology Conference, Purdue Research Foundation, 1980.

10. Giacomelli, I. E., and Giorgetti, M., "Investigation on Oil Stiction in Ring Valves," Quaderni Pignone, 20 (1975), Italy.

11. Boyce, W. E., and DiPrima, R. C., Elementary Differential Equations and Boundary Valve Problems, 3rd ed., John Wiley & Sons, New York, NY, 1977, p. 535.

12. Thomson, W. T., Theory of Vibration With Applications, 2nd ed., Prentice Hall, Englewood Cliffs, NJ, 1981, pp. 323-325.

13. Thomson, pp. 218-221.

14. _____, ANSYS 4.2, Swanson Analysis Systems Inc., Houston, Pennsylvania.

15. Pestel, E. C., and Leckie, F. A., Matrix Methods in Elastomechanics, McGraw-Hill, New York, NY, 1963.

16. Mabie, H. H., and Ocvirk, F. W., Mechanisms and Dynamics of Machinery, 3rd ed., John Wiley & Sons, New York, NY, 1975, p. 19.

APPENDIX A: The Experimental Setup

The schematic of the experimental setup is shown in Fig. A.1. A complete list of the equipment is shown below. (The numbers in the list correspond to the number shown in Fig. A.1):

1. Compressor:

   Manufacturer: Ingersoll Rand Two Stage Air Compressor

   Model: 242-Two-stage air compressor

   S/N (serial number): 493670

2. Proximity Probes Used to Measure Valve Position:

   Manufacturer: Electro Corp.

   Model: 4947F Electro Mike Sensor

   Quantity: 4 (one for each point measured)

3. Electronics to Decode Signal From the Proximity Probes:

   Manufacturer: Electro Corp.

   Model: PA12D47 Electro Mike Displacement Transducer System

   Quantity: 1 (same system used for all probes)

   S/N: 607428

4. Pressure Transducer Measuring the Outlet Plenum Pressure:

   Manufacturer: PCB

   Model: 111A27-62 Piezoelectric Pressure Transducer

   Serial Number: 607

5. Outlet Pressure Transducer's Conditioning Amplifier:

   Manufacturer: PCB

   Model: 480D09 Power Unit

   Serial number: 438

6. Pressure Transducer Measuring the Cylinder Pressure:

   Manufacturer: PCB

   Model: 111A26 Piezoelectric Pressure Transducer

   Serial number: 2773

7. Cylinder Pressure Transducer Signal Conditioner:

   Manufacturer: PCB

   Model: 480D09 Power Unit

   Serial Number: 439

8. Digital Oscilliscope:

   Manufacturer: Norland

   Model: 3001 Processing Digital Oscilliscope

   Serial Number: 0134

9. Data Acquisition System:

   Manufacturer: DEC

   Model: PDP 11/23-AX Data System

   Serial Number: WM 820121089U

10. Data Acquisition System Terminal:

Manufacturer: DEC

Model: 440 WF GIGI Terminal

Serial Number: WF 11341

11. Terminal Monitor:

Manufacturer: GBC

Model: MV-12 Closed Circuit Monitor

Serial Number: S8002

12. Computer Where Simulation Program Was Executed

Manufacturer: DEC

Model: VAX 11/780 computer

As the schematic of the experimental setup shows (Fig. A.1) the proximity probes were used to measure the valve position. These proximity probes emit a low level radio frequency field in front of the sensor. As a metallic material approaches the sensor, the characteristics of the field change and the change can be decoded by electronics to yield a voltage. This voltage can then be multiplied by a sensitivity factor to yield the position of the body being monitored. Since the proximity probes were mounted in the cylinder head, the cylinder head was made out of aluminum, a non-ferrous material. The valve positions could then be measured without substantial interference from the cylinder head. In some instances the sensors were mounted in the cylinder head such that aluminum completely surrounded the sensor. Those sensors had to be recalibrated since the

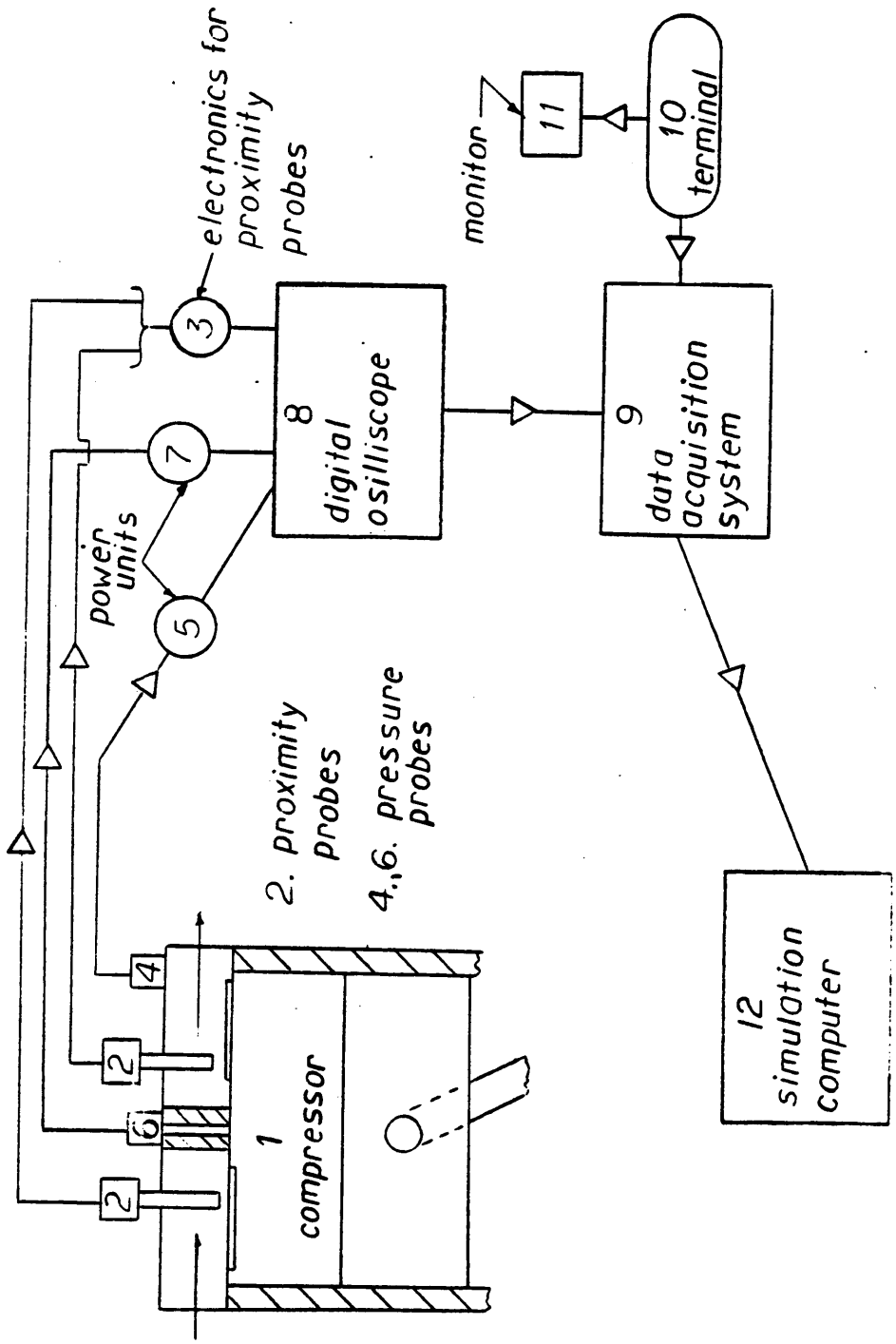

Figure A.1: The experimental setup.

manufacturer's sensitivity measurements were performed with the sensor surrounded by air.

As shown in Fig. A.1, the cylinder pressure was measured using piezoelectric pressure transducers. It was found that the driving motor transmitted 60 Hz noise to the pressure transducer. To eliminate this noise the pressure transducers were isolated from the compressor by Teflon adapters.

The analog signals from the transducers and probes were signaled averaged and digitized using a digital oscilliscope using 150 samples at a sample rate of 200 μs. Then using a RS 232 data link and an interface program, the data was transferred from the digital oscilliscope to a data acquisition system for storage (Fig. A.1). The data was then copied from the data acquisition system to the simulation computer for future comparisons with analytical results.

The vita has been removed from the scanned document